Modelling Lyman-α Emission from Star Forming Galaxies at High Redshift Using Cosmological Simulations

Espen Hodne

Thesis submitted for the degree of
Master of Science in Astronomy

Institute of Theoretical Astrophysics
University of Oslo

01.06.2019

Abstract

I study Lyman-α emission from high-redshift galaxies using the high-resolution smoothed particle hydrodynamics (SPH) galaxy simulation "Ponos" at redshift $z = 6.5$. The focus of my study is the luminosity from hydrogen recombination and the corresponding surface brightness.

I calculate an intrinsic luminosity for the galaxy using parameters from the simulation; as well as a self-shielding scheme that neutralizes all gas where temperature $T < 10^4\,\mathrm{K}$ and hydrogen number density $n_\mathrm{H} > 0.1\,\mathrm{cm}^{-3}$. The data is then interpolated onto a grid, where I apply ionization from active galactic nuclei and radiating stars.

I make some general observations and calculations about the galaxy simulation as a whole, before reducing my study to a $50 \times 50 \times 50\,\mathrm{kpc}$ box around the main dark matter halo in order to do more detailed observations of the area encompassed by and immediately surrounding its 21.97 kpc virial radius. The final Lyman-α luminosity found in this area is $7.68 \times 10^{43}\,\mathrm{erg\,s}^{-1}$. The emission is sent through a scattering scheme in order to give a more realistic image of the galaxy. Finally I make Lyman-α surface brightness maps, surface brightness profiles and spectra as seen from six directions. The scattering smears out the Lyman-α radiation, giving larger and more extended maps, better representing observations. The accompanying spectra shows peaks at blue- and redshifted wavelengths. Doppler shifted photons have a smaller chance of scattering, making them more likely to escape. The high values in the center of the spectra represents scattering in the less dense outskirts of the galaxy.

I make comparisons to galaxies at redshifts $5 < z < 6$, as well as to giant Lyman-α nebulae. The findings are that the surface brightness profile is around two orders of magnitude larger than for typical galaxies at similar redshifts, and more akin in values to the observed superluminous Lyman-α nebulae.

My findings indicate that the main reason of this high luminosity is the large star formation rate of $42.41\,\mathrm{M}_\odot\,\mathrm{yr}^{-1}$. This is the result of an ongoing starburst, starting approximately 150 million years before redshift $z = 6.5$. I postulate two possible reasons for this starburst: i) it is due to lack of feedback from the AGN, or ii) the simulation is experiencing a galaxy. The latter is the most likely due to the main galaxy's proximity to another galaxy.

Acknowledgments

First and foremost I want to thank my supervisors, Peter and Sijing. They help they have given has been invaluable and this thesis would not in any way have been possible without them. This also extends to the entire extragalactic astronomy group at ITA, who have never held back on help and input whenever I have asked.

My second thanks goes to the student communities I have been a part of througout my degrees. First of all Fysikkforeningen and Lillefy. You made sure my bachelor degree was one of the best periods of my life. I also want to thank AFU and Stjernekjelleren, for the student community, activities and laughs throughout the stressful period which is the masters degree. A special thanks here goes to Renate, who have for almost the entirety of my studies been there to help whenever I have been struggling with physics, math or programming.

Next, I want to thank my Dungeons & Dragons group. It was started during the first bachelor semester, and has been going strong since. Thank you Marius, Stian, Fredrik, Reidar, Joseph, Marianne and Andreas for giving me one evening per week to delve into a whole other world along with you.

As for my family, I want to thank my mother and father for always supporting me, even though I moved far away. This also goes to my grandmother, for her support of a sometimes poor and lost student.

Lastly, I want to thank everyone else not specifically mentioned here. These have been five years of hard work and little sleep, but also five years of fun conversations, parties, events, balls, cabin trips and more. So a huge thank you to all the students and personell who has made this possible, and given me the best years of my life.

Contents

List of Figures

Chapter 1

Introduction

A long time ago, in a simulated galaxy far far away...

In the present day, galaxy simulations is one of the prime ways to study galaxy formation and properties. For my master's degree in astronomy, I have been analysing the Ponos high-redshift simulation. This simulation was performed using the smoothed particle hydrodynamics (SPH) code GASOLINE, which uses a particle-based system to study the galaxy.

Lyman-alpha radiation, hereafter shortened to Lyα, is the most abundant radiation of those emitted by hydrogen atoms. This makes it an excellent probe for the early Universe, as the Lyα lines from that time are still quite strong. Since the early Universe consisted mostly of hydrogen, with a relatively low amount of dust and metals, Lyα radiation is thought to give an accurate image of galaxies. This goes especially for the early galaxies, whose gas consisted almost exclusively of the Lyα-emitting kind.

Lyα can be found practically everywhere in the Universe. The two main sources are interstellar nebulae in galaxies themselves, as well as gas around and in between galaxies. These are called interstellar- and circumgalactic media, and will from here and out be shortened to ISM and CGM. Lyα photons are made when an ionizing source - often light emitted from stars - ionizes these gas pockets. Portions of the gas will then recombine and emit Lyα photons.

In this thesis I look at the mechanisms behind the Lyα radiation, as well as its sources. Then I replicate this numerically, to calculate Lyα emission from the Ponos simulation. This forms a model for Lyα emission from numerical galaxies made with smoothed particle hydrodynamics. The goal is to see whether my results are comparable to the observed data from similar high-redshift galaxies, and thus test the realism of my model and the original simulation itself.

Beyond the introduction, this thesis has four more sections. In the theory sections I discuss the mechanism behind Lyα creation and radiative transfer, as well as its sources. I also look at early galaxies as a whole, how they form, and how ionization from stars and active galactic nuclei (AGN) affect the Lyα generation.

In the methods section I look at the numerical methods used, the different programming schemes, formulae and approximations. I also give an introduction to the Ponos

simulation.

Thereafter I present my results. These include the Lyα emission, surface brightness, distribution of hydrogen based on temperature and density as well as Lyα radiative transfer. I include the intrinsic properties of various galaxy parameters as well as the Lyα luminosity, how the luminosity looks after I have made approximations and ionisations, and the radiative transfer. I will also look at how the Lyα luminosity differ based on the resolution used.

Finally discuss my findings and results. I will talk about the resolution, self-shielding, ionization from internal sources and what the radiative transfer does to the Lyα luminosity. I then conclude with the main findings, and suggest future work that can be done in the field.

Chapter 2

Theory

2.1 Early Galaxies

The following section is based on the book *The First Galaxies in the Universe* by Abraham Loeb and Steven R. Furlanetto; and from the course I had in extragalactic astronomy, lectured by Sijing Shen.

In this thesis I look at high-redshift galaxies. This is synonymous with galaxies that existed in the early Universe. These galaxies are notable for several reasons, the arguable main reason that they can be considered more "pure" than later galaxies. This means having very low metal contents and mostly consisting of hydrogen and helium. While this in a way rings true for all galaxies, the early ones have experienced far fewer supernovae and neutron star collisions that would create and distribute these heavier elements.

First and foremost, one may ask the question: what is a galaxy? In simple terms, a galaxy is a collection of matter, bound together by gravity. Unlike intergalactic gas clouds, a galaxy is a distinct gathering of materials, much denser than the clouds. The three main "ingredients" of a galaxy is dark matter, gas and stars. Other commonly found objects are planets and dust, but planet masses are negligible compared to stars, and in the early galaxies the dust is minimal. Therefore I will focus on dark matter, gas and stars.

Let us look at a sample very early Universe consisting of dark matter and gas. This will be mostly uniform, but here and there a density perturbation will happen, which, if large enough, can lead to structure formation. A galaxy forms when dark matter gathers in an area, and then collapses due to its own gravity. The mass of this structure is called the "virial mass", and resides within the "virial radius". The matter within and close to this virial radius is what I will look at in this project. The force counteracting this collapse is the very expansion of the Universe itself. The Universe expands in all points of space, and acts as a force pushing particles apart, while their gravity pulls them together. If the gravity proves stronger, we will gain a *dark matter halo*; a stable structure with strong enough gravitational pull that the expansion of the Universe will not push it apart.

The gas in the Universe interacts gravitationally with the dark matter, it will be pulled into the virial radius along with the dark matter. Unlike the dark matter, gas is subject to hydrodynamic forces. It interacts with itself, and the particles will exert pressure onto one another. This pressure is higher the warmer the gas is, so too high temperatures will prevent the gas cloud from collapsing into the halo. However, if the gas cools enough, it will collapse, and we will have a galaxy consisting of dark matter and gas. The mass required for gas, or baryonic matter, to collapse is called the *Jeans mass* (after British physicist Sir James Jeans).

So, essentially, we have warm gas that is losing energy due to radiating it away. While gravity pulls the gas together, gas pressure and radiation from itself will push it apart. If gravity wins this tug of war, and the gas becomes cold enough, it will clump together and make a star forming region.

Now we have gas concentrated in a relatively small zone, along with dark matter. If parts of this gas cools even further, the Jeans mass of the gas filaments will continue to decrease. When it reaches the mass scale of a singular star, things start happening.

If we look at galaxies like our own milky way, the interstellar medium (ISM) will have an abundancy of heavy elements such as carbon and oxygen. For the formation of the first stars, however, these heavy elements did not yet exist. The galaxies consisted almost exclusively of hydrogen and helium. As the temperature cools down to $T = 10^4\,\mathrm{K}$, the atoms lose energy, collisions are weaker and single-atom hydrogen does not emit radiation. This leaves it unable to cool further, and get cold enough to collapse into stars. However, we also had molecular hydrogen, that is, hydrogen atoms that had bound together to form molecules. Even though on a cosmic scale this molecular hydrogen was negligible compared to atomic hydrogen, it was still sufficiently enough electrons in the star forming gas to catalyse the H_2 and cool it down to earth-like temperatures. All in all, this was enough to make the gas cold enough to form the first stars.

I am skipping over a lot of details here. Star formation is a field in itself, that I will not delve further into. However, now that the gas was cool enough to form stars, these first, simple stars created metals. These metals allows for gas cooling down to well below $10^4\,\mathrm{K}$, which lets the next generation of star formation create lower-mass stars. These new, smaller stars are of the same type we see in galaxies today; like our own sun.

2.2 Lyman-Alpha Radiation

Lyman-alpha radiation, or Lyα for short, is one of the most abundant kinds radiation in the Universe. The main source of the radiation is recombination of hydrogen. In 1967, Partridge & Peebles [11] predicted that the Lyα line could be a way to find star-forming galaxies at very large distances. This is based on the assumption that young, new stars would emit a huge abundance of ionizing photons, in which most would be reprocessed into recombination lines. Due to the nature of the interstellar medium, consisting mostly of hydrogen gas, most of the recombination lines should be Lyα lines.

Table 2.1: List of the spectrographic notation of the first four orbital quantum numbers.

Orbital number l	Letter
0	s
1	p
2	d
3	f

This has been proven during the last two decades, and as per 2015, we have been able to observe Lyα emitting galaxies of up to redshift $z = 8.68$ [12].

Lyα transition has also been extremely useful in observational cosmology. Studies of the Lyα forest in quasar spectra has allowed us to very accurately measure the matter distribution throughout the Universe. The Lyα forest is a very useful observational tool for the parts of cosmology on scales that are not viewable through galaxy surveys and/or Cosmic microwave background (CMB) radiation.

So why is Lyα radiation so abundant? First and foremost, the primary source of Lyα radiation is recombination of hydrogen. Since hydrogen is by far the most abundant gas in the Universe, and is relatively easy to ionize, it stands to reason that radiation from hydrogen transitions should be common.

To study how we get Lyα radiation from hydrogen, we look at the radiative transfer mechanisms.

2.3 Radiative Transfer

This section is based on *Physics of Lyα Radiative Transfer* by Mark Dijkstra (2017) [1].

2.3.1 Radiative Hydrogen Transitions

In order to fully understand the Lyα emitting sources we need to study radiative transfer. We need to look at the quantum physics of electron levels.

In quantum mechanics, an electron is described by a wave function $\psi(\mathbf{r})$. This wave function describes the probability of finding the electron in location $\mathbf{r}$. Without going into further detail as to the physics behind the wave function, what is important to us are that this function is fully characterized by two quantum numbers: the principal quantum number n and the orbital quantum number l, where l is limited by only being able to take the values $l = 0, 1, 2, ..., n - 1$.

Classically, to describe a state, one uses a combination of the quantum numbers, with the syntax (n, l). I am changing the syntax a bit, so the l portion will be given a different notation - the "spectroscopic notation", as shown in table 2.1. This means $n = 1$ can only have $l = 0$, and the notation would thus be the "1s"-state. Similarly, for the second energy level, the electron can exist in the "2s"- and "2p"-states.

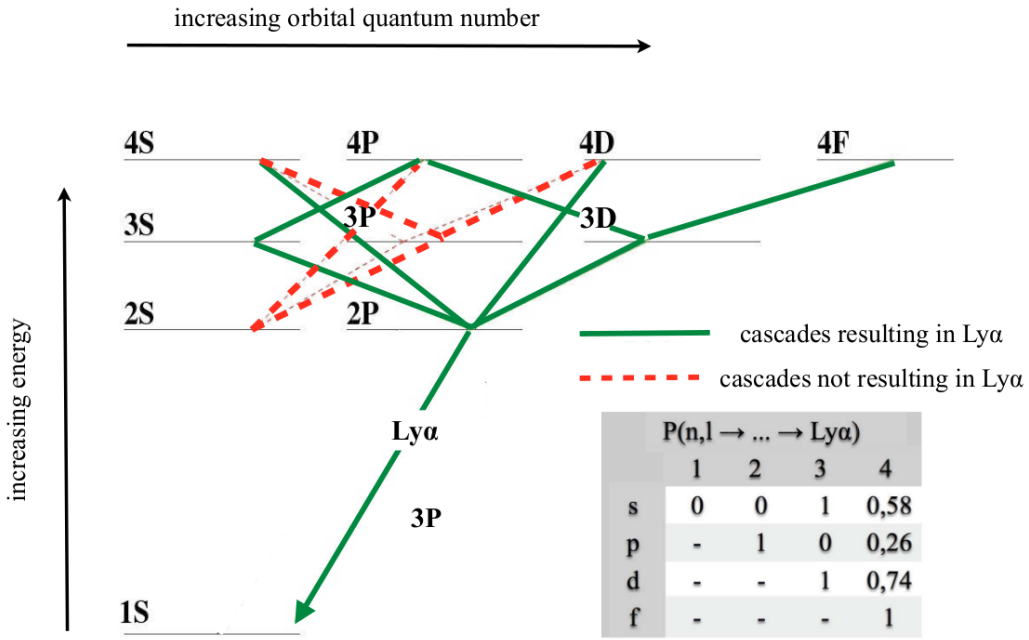

Figure 2.1: The Lyα cascade, illustrated. Adapted from [1].

When an electron goes to a lower energy level in an atom, it will release the energy in form of a photon. The energy lost, and thus wavelength of the photon, changes based on the starting and ending levels of the drop. This drop, or transition, is given a different name based on the principal quantum numbers involved. When an electron de-excites to $n = 1$, we get the **Lyman series**. De-excitation to $n = 2$ would be the **Balmer series**, and so on. As for the α-part, we look at where the electron transitions from. If it falls from $n = 2$ we get Lyα. Had the transition been from $n = 3$, it would have been Lyβ. From $n = 4$ it would have been Lyγ etc.

As is usually the case with quantum mechanics, which transitions will happen is governed by probabilities. A transition can only happen at a difference of $|\Delta l| = 1$ at a time. A series of these transitions can be called a "cascade", in which some will result in a Lyα photon being radiated. Most electrons will end their cascades in either the 2s or the 2p state. Transition from 2s $\rightarrow$ 1s is a so-called "forbidden" transition, meaning that it has a very low chance of happening, and can thus be neglected. The 2p electrons will however move into 1s, giving us a Lyα photon. If we start at $n = 4$, we get that 58% of the de-excitations result in Lyα radiation.

This is illustrated in figure 2.1. This shows the probabilities of getting a Lyα photon from any given relevant quantum state.

So, to summarize, the reasons we see so much Lyα is:

1) The high abundancy of unionised hydrogen gas near luminous sources.

2) The high number of hydrogen transitions that results in a Lyα emission.

2.3.2 Hydrogen Excitation and Ionization

Now that I have covered how an excited hydrogen atom emits Lyα radiation, I will talk a bit about how the atom gets so excited it just can't hide it in the first place.

In general, there are two ways an atom can end up in an excited state. First, there are **collisions**, in which case the electron starts out bound to the atom. Secondly, there is **recombination**, where the electron comes from an external source.

In general, we can look at two "cases" when it comes to the de-excitation; "Case-A" and "Case-B". Case-A is a very general case, in which electrons and protons can recombine into *any* state (n, l) and we allow all non-forbidden transitions. Case-B, which is what I use in this project, has two requirements: 1) we do not allow for recombination directly into the ground state, which would produce an ionizing photon; and 2) we neglect radiative transitions of the higher order Lyman series, that is, anything besides Lyα.

Case-B is often used in astrophysics, since it represents a more realistic environment. In most astrophysical gases, higher order Lyman series photons would simply be re-absorbed, along with the ionizing photons. Thus, this radiation is not actually much present in a real gas.

Collisions

A collision is in this case an interaction between an electron and a hydrogen atom. An electron will "hit" the hydrogen, and the kinetic energy between the incoming and bound electrons will, in simple and not quite physical terms, knock the bound electron to a higher orbit, in what we call an excitation. The incoming electron does not always have enough energy to free the bound electron entirely, though, and might just push it into a higher orbital. Regardless, this works as a set-up for a de-excitation later on, which can produce a Lyα photon.

The details and calculations, however, are a bit more complicated. First of all, how efficient this process is depends on the relative velocities of both involved parts. Since we are talking about an insanely large amount of particles, doing the calculation for every single particle is unfeasible. We therefore use statistical distributions. Therefore the collisional Lyα production will include a product of both species' number density, along with the rate coefficient $q_{1s2p}(P[v_e])$. Here $P[v_e]$ denotes the electrons' velocity distribution. If we assume a Maxwellian velocity distribution for the electrons, $P[v_e]$ will only depend on the temperature T. Thus the rate coefficient will be a temperature dependant, $q_{1s2p}(T)$. The total Lyα production rate from collisional excitation will then be

$$R_{\text{coll}}^{\text{Ly}\alpha} = n_{\text{e}} n_{\text{HI}} q_{1\text{s}\to 2\text{p}}\,\text{cm}^{-3}\text{s}^{-1}, \tag{2.1}$$

where n_{e} and n_{HI} are the number densities of electrons and neutral hydrogen; and q is the collisional excitation rate coefficient.

Calculation of collision strength is in general a very difficult process, since for the interesting free electron energy, the free electron will spend a (relatively) long time near

the target atom. This will cause distortions in the bound electron's wave function, which may cause very complex quantum mechanical interactions. This becomes more and more prominent as n increases, and is most reliable when $1s \rightarrow nl$, where $n < 4$ and $l < d$.

The radiation these collisions produces will reduce the gas' thermal energy. This energy loss, or cooling, per unit volume is given by

$$\frac{dE_{\text{th}}}{dVdt} = n_{\text{e}} n_{\text{HI}} C(T), \tag{2.2}$$

where E_{th} is the thermal energy, t is time, V is volume, ne and n_{HI} are the number densities of electrons and neutral hydrogen; and $C(T)$ is the cooling rate per hydrogen nucleus obtained from collisional hydrogen excitation into states of $n \leq 4$. $C(T)$ can be expressed as

$$C(T) = \sum_{u} q_{1\text{s}\rightarrow\text{u}} \Delta E_{1s\rightarrow u} \text{erg}\,\text{cm}^3\,\text{s}^{-1}, \tag{2.3}$$

where "u" is all excited states, q is the collisional excitation rate coefficient and ΔE is the energy difference between the states.

The sum is over the all excited states u. At temperature $T = 10^4$K the cooling rate starts increasing immensely, as seen in figure 5.2. This reflects the strong temperature dependence of the fast-moving electrons, the ones that can excite hydrogen atoms.

The cooling rate per unit volume depends on the product of $C(T)$, n_{e} and n_{HI}. Therefore we have a dependency on the ionization state of the gas. If we assume collisional ionization equilibrium - that is, that the ionization state is entirely depending on temperature - the cooling rate per volume will only be a function of temperature.

Recombination

A recombination is when a free electron combines with an atom and fills up a "hole" in the atom's "electron shells". This electron is rarely absorbed right into the ground state, however, but in a quantum state (n, l). It will then radiatively cascade down to the ground sate $(1, 0)$, emitting radiation along the path.

The probability of getting a Lyα photon from the cascade following a recombination is given by

$$P(n, l \rightarrow \text{Ly}\alpha) = \sum_{n',l'} P(n, l \rightarrow n', l') P(n', l' \rightarrow \text{Ly}\alpha). \tag{2.4}$$

Here n' and l' are the intermediate states. This equation basically tells us the probability of moving from one state in the cascade to the next, as figure 2.1 illustrates.

If we shorten it down, we can write the probability for getting a Lyα photon as

$$P(\text{Ly}\alpha) = \sum_{n_{\min}}^{\infty} \sum_{l=0}^{n-1} \frac{\alpha_{nl}(T)}{\alpha_{\text{tot}}(T)} P(n, l \rightarrow \text{Ly}\alpha). \tag{2.5}$$

The first term denotes the fraction of recombination events into the (n, l) state, and $\alpha_{\rm tot}(T)$ is the total recombination coefficient.

In this project, I assume that Case-B recombination is in effect at all time. Thus the utilized recombination coefficient will be $\alpha_{\rm B}$.

2.4 Lyα Sources

The following section is based on chapter 5: Astrophysical Lyα Sources in *Physics of Lyα Radiative Transfer* by Mark Dijkstra (2017) [1].

As previously mentioned, Lyα radiation can be found just about everywhere in the Universe. As we have discussed, it originates from collisions and recombination of hydrogen. Thus it stands to reason that for an abundance of Lyα radiation to be created, we need a large reservoir of hydrogen gas. For continuous emission, it should be near an ionizing source. Cooling of cold gas will also emit Lyα, while cooling of hot gas will emit X-rays, and is thus uninteresting to us.

The radiation has two main sources, which I will now give a closer look: **interstellar HII regions** and **circum/intergalactic media**.

2.4.1 Interstellar HII Regions

The greatest Lyα source in the known Universe is interstellar HII regions. These are regions of interstellar medium close to hot and young stars. These stars are massive, and produce plenty of photons to ionize the hydrogen gas around them. The gas will then sporadically recombine, and emit Lyα photons. We call the lines from this phenomenon "nebular lines", and they include both Lyα and Hα. A good example is the Orion nebula, which can be seen with the naked eye in the Orion constellation. The beautiful red light we see are in the visual spectrum, and comes from Hα radiation. However, if we look at the probability of a case-B recombination emitting a Hα photon, we get $P(H\alpha) \sim 0.45$, compared to $P(Ly\alpha) = 0.68$. This will give a flux of about 8 times more Lyα emission in comparison. So even if the constellation is already this bright in the visible spectrum, if we moved over to the Lyα spectrum at 1215.67 Å, the visibility would increase by almost an order of magnitude. This should give an indication of how bright Lyα is, and why it is so useful for observations.

Since these regions are around hot stars, there is a constant tug of war between ionization and recombination. This will lead to some sort of balance, in which the recombination rate will be in an equilibrium. It should be noted that this equilibrium is only satisfied in ordinary, non-expanding HII regions. The recombination rate of this equilibrium region will equal the nebulae's total photoionisation rate, that is, the total rate at which the HII region absorbs ionizing photons.

A way to find Lyα luminosity from this region is through the "initial mass function", or IMF. Several models for this exist, and the Ponos simulation, which I analyse, use the so-called Kroupa IMF [13]. With this IMF, the luminosity should be around

$$L_\alpha = 1.7 \times 10^{42} \times \mathrm{SFR}(\mathrm{M}_\odot/\mathrm{yr})\,\mathrm{erg\,s^{-1}} \ \text{(Kroupa, } Z = Z_\odot) \tag{2.6}$$

In section 5.1.1 I compare my findings to the results from the Kroupa IMF.

2.4.2 The Circum- and Intergalactic Media

In addition to the nebulae, we also have Lyα emission from circumgalactic and intergalactic media. This is mostly from the CGM, as it is being continuously lit up by the galaxy it surrounds. This will ionize the gas, which will then produce Lyα radiation the same way as the interstellar medium. The IGM, however, is a mix of emission and absorption. For the most part, the IGM is an absorbing phenomenon, and generates what is known as the Lyα forest.[1] However, there is no clear line between the CGM and the IGM, and filaments of the IGM could in principle emit Lyα photons from cooling. However, for most practical reasons, the IGM is not a Lyα emitter, while the CGM is.

There is also collisional emission happening in the CGM, inside the self-shielded regions of the clouds. This is a very temperature-dependant procedure, and is proportional with $\propto e^{-E_{\mathrm{Ly}\alpha}/k_{\mathrm{b}}T}$. Because of the way I do self-shielding in my model, this production will be negated in the densest, coldest areas of the gas.

There are two main differences between Lyα emission from CGM and from the interstellar regions:

i) The Lyα emission from the CGM comes from a spatially extended region. Technically the emission from the interstellar regions does as well, but since the galaxies are so far away, the ISM regions within the galaxy may appear like point sources to us. Therefore, instead of looking at flux, it is better to look at the surface brightness of the extended area. This will tell us how much is emitted at each point, and is essentially flux over a solid angle. Figure 2.2 illustrates the geometry, along with giving us the equation

$$S = \frac{\text{Flux}}{d\Omega} = \frac{d_{\mathrm{A}}^2(z)\text{Flux}}{dA} = \frac{d_{\mathrm{A}}^2(z)}{dA}\frac{\text{Luminosity}}{4\pi d_{\mathrm{L}}^2(z)}, \tag{2.7}$$

where dA is the surface of our object, $d_{\mathrm{L}}(z)$ is the luminosity distance to redshift z and $d_{\mathrm{A}}(z)$ is the angular diameter distance to z. The relations used were that the solid angle $d\Omega$ can be defined as $d\Omega \equiv \frac{dA}{d_{\mathrm{A}}^2(z)}$ and that $\text{Flux} = \frac{\text{Luminosity}}{4\pi d_{\mathrm{L}}^2(z)}$. Using $d_{\mathrm{L}(z)} = d_{\mathrm{A}}(z)(1+z)^2$, I rewrite the expression to

$$S = \frac{1}{dA}\frac{\text{Luminosity}}{4\pi(1+z)^4}. \tag{2.8}$$

Equation 2.8 is instrumental for making the surface brightness profile, as seen later in the thesis.

ii) Lyα from CGM comes from external sources. The source of illumination does not come from the gas itself, but instead from the galaxy it surrounds and background

[1] The Lyα "forest" happens when Lyα radiation hits pockets of neutral gas in the IGM and is absorbed, creating a dark line in our telescopes. As the photons are being continuously redshifted moving through the Universe, a plethora of absorption lines will be made in the spectrum. The remaining light will then look like a forest.

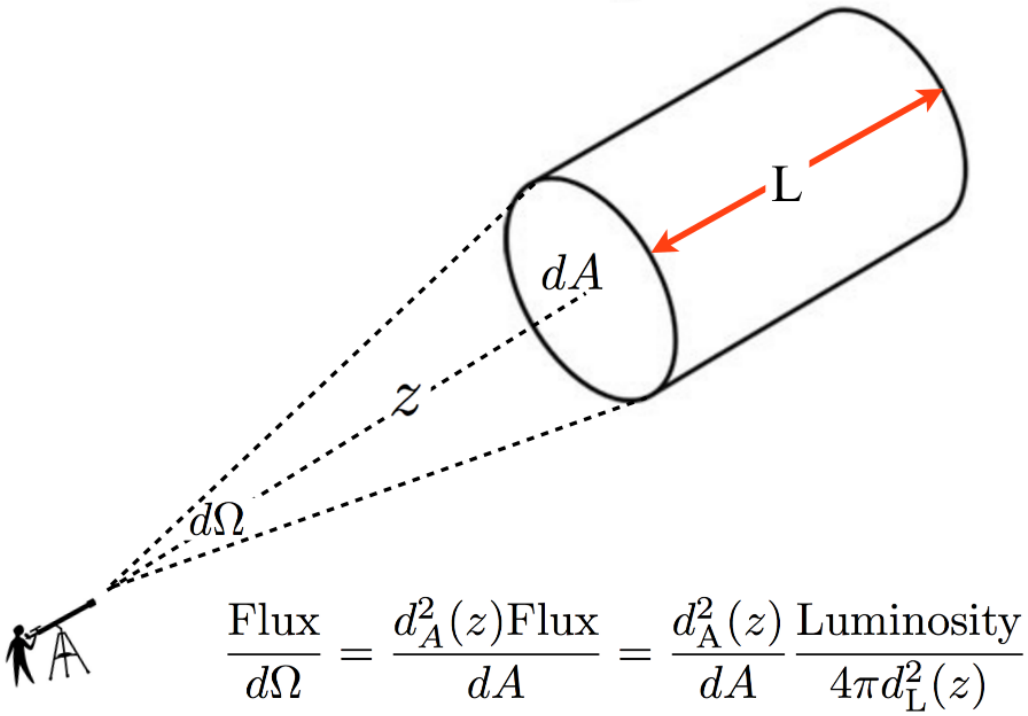

Figure 2.2: Geometric presentation of how we look at surface brightness, along with formula for obtaining it from the flux. Figure adapted from [1]

.

fields. One of the ways the CGM/IGM can be ionized is through *fluorescence* [14] [15], which is a phenomenon where a material absorbs radiation of one wavelength and emits radiation of another. This fluorescence will stop once the external source is removed or depleted. For Lyα, the fluorescence comes from the recombination cascade; where Lyα radiation will be one of the emitted wavelengths.

2.4.3 Summary

To summarize: Lyα luminosity is generated by two main methods, in two main dominions of space.

For the methods, we have recombinations and collisions. Recombination comes from when a free electron recombines with a free proton, and will then de-excite and have a significant probability of emitting a Lyα photon as part of the emitted "cascade". With collisions, a nearby free electron will collide with a neutral hydrogen atom, and will then electromagnetically "push" the bound electron to a higher orbit. This electron will then de-excite, and likely emit a Lyα photon. This is also known as "cooling".

The dominions in which this happen are two; first there is the interstellar medium inside the galaxies, where recombination reigns supreme. This part of the galaxy is in constant heated turmoil, being close to ionizing stars. Cooling also happens here, but the luminosity it produces is a small fraction of the recombination luminosity. Outside the galaxies we have the circum- and intergalactic media. There is no clear border between these, as they "bleed into" one another, but in general the CGM is much more luminous than the IGM. The CGM is being heated from the galaxy it surrounds, while the IGM mostly has to rely on background fields. These areas are fluorescent, meaning that if the source of ionization was to disappear, they would go dark almost instantly.

2.5 Lyα Resonant Scattering

As a Lyα photon moves through a galaxy, it has two possible fates. It can escape or be destroyed.

On the way to either of those fates, the Lyα photon will typically face many obstacles along its way. Most of these obstacles will be hydrogen atoms, and a few will be dust particles. These are much larger than a single hydrogen atom, but still small enough to be microscopic and retain some quantum mechanical properties in their interactions with the photons.

In this section I will follow the journey of a single Lyα photon through a galaxy.

First, the photon is emitted in a random direction. This is in an ionizing zone, so there are plenty of ionized hydrogen atoms around it. The photon looks around for atoms to scatter off of, but finds none. This is not because there are no atoms around, but because the cross-section of the atoms do not match the wavelength - $\lambda = 1216$ Å - of the Lyα photon. Each kind of atom has a cross-section σ which "matches" a certain wavelength. The further the photon is from the atom's resonant wavelength, the lower the chance of interaction. This is the reason the Lyα photon will simply "pass through" (to use a classical image on a quantum mechanical phenomenon) the ionized hydrogen

and all the helium atoms it encounters; the cross-section is such a bad match for the photon frequency that it will not interact. However, after a little while, our photon encounters an HI atom.

Now this particular atom is very quiet and still-standing, so our little Lyα photon will just be absorbed, and re-emitted in a random direction. This is what is usually referred to as a "scattering", but can be thought of as "absorption and re-emission". This happens over a very short period of time (10^{-8}s), and the re-emitted photon retains some properties of the absorbed photon. It is important to keep in mind that this is a quantum-mechanical phenomenon, and it thus does not follow the Newtonian collision laws. Therefore it can bounce off all directions, governed by a so-called "phase function". This phase function will differ depending on if the frequency matches the photon spot-on, in the "core" [16], or whether it lands on of the cross-section's "wings" [17]. In general, though, the photon will have a greater chance of being scattered forwards or backwards relative to its current direction.

So let us say that our photon gets scattered backwards, and on its way it crosses paths with a fast-moving HI atom. Since this atom is moving, its cross-section σ will be Doppler-shifted to a different resonance frequency. This means that for an outside observer, the probability of an interaction has been shifted to a higher red- or blueshift, depending on direction of the atom's movement. However, this is the case only for photons moving along the same direction as an atom. From the photon's point of view, only the parallel motion will be shifted, and not the perpendicular one. This means our little photon hits a fast-moving atom perfectly in the flank, and resonates with its (from the photon's point of view) unchanged wavelength. This is where the fun begins.

The photon is now, for a very short while, being absorbed by the atom. Since the atom is moving at a very high velocity, the re-emitted photon will - depending on the direction of the re-emission - be Doppler shifted. If it is emitted in the same direction the atom is moving, it will be blueshifted and have gained energy, and if it is emitted away from the atom it will be redshifted and have lost energy. This is is illustrated in figure 2.3.

Now, our photon decided to go along the same direction as its new friend, and has been heavily blueshifted. This means its wavelength is no longer $\lambda = 1216$ Å from our point of view, and it has a very low chance of interacting with still-standing HI atoms. This means it can do large leaps in distance throughout the galaxy without colliding with anything. It is at this point the photon is most likely to escape from the galaxy, and therefore most escaped Lyα photons we see will be red- or blueshifted. This can be seen in the Lyα spectra in figures 4.6 through 4.9. Escape, however, is not guaranteed. After a long jump, the photon can still collide with either an HI atom or a dust particle.

As for HI, there are generally two possibilities. Either, our friend the photon will hit a high-velocity atom, with a cross-section attuned to its new wavelength [2]. The other possibility is that it is simply snatched up by a more still-standing atom. Let us assume that our photon's blueshift is massive; so it is very far out on the wings of a

[2]That is, an atom that moves such that the photon is Doppler shifted back to near-1216 Å in the atom's reference frame.

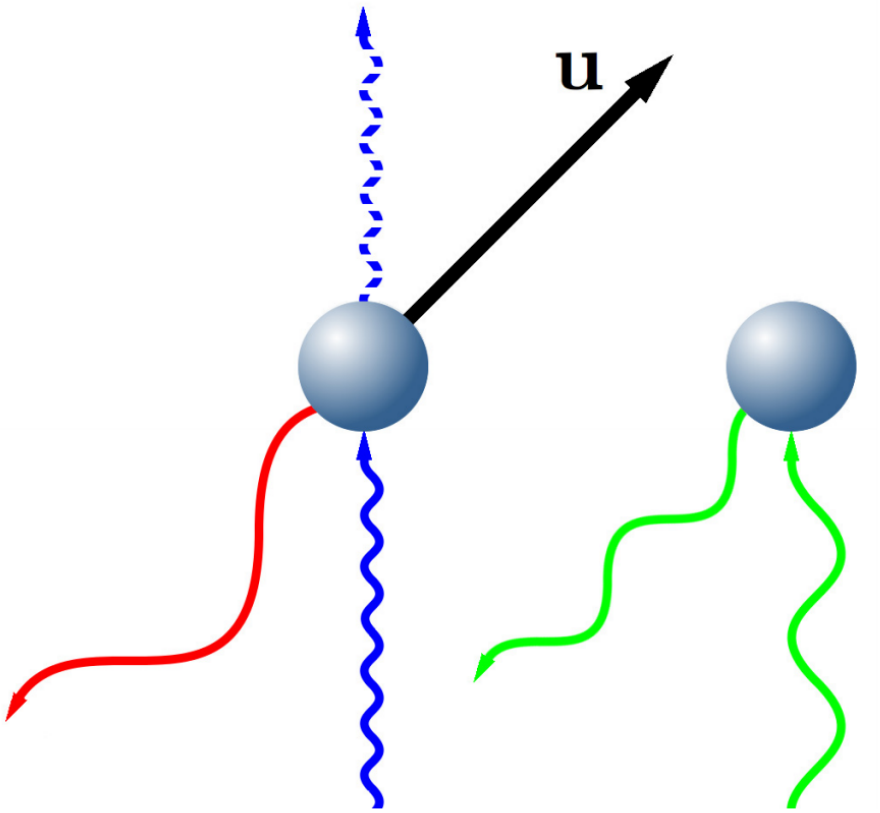

Figure 2.3: Illustration of the frequency shift of a scattered Lyα photon. To the *left* we see the scattering as an external observer. In this point of view, the photon is exiting in negative direction of the atom's movement, and is thus redshifted. The exception is if it happens to be scattered the same direction as the dashed blue line, in which case its frequency will be unchanged. To the *right*, we see the scattering from the atom's reference frame. In this frame it is an ordinary scattering that does not change the photon's properties. Adapted from [2].

quiet HI atom cross-section. This means there is a exceedingly low chance of scattering off the slow photon, but the probability is still non-zero. In fact, there are so many more slow than fast-moving atoms in the galaxy that for the highly shifted photons, the chance is actually larger to be absorbed into a slow atom than finding a fast-moving one [2]. When scattering against slow-moving atoms, the photon will have a tendency to drift towards its line center [18]. This means that once our friendly photon hits a slow-moving atom, it will tend to be shifted back towards wavelength $\lambda = 1216$ Å. It is thus be more likely to hit more slow-moving HI atoms. This means the jumps get shorter and shorter, and its chances of escaping the galaxy decreases. Its escape attempt foiled, our photon must now be happy with short bounces between the slow atoms, until it happens to catch a fast-moving atom again or hit a dust particle.

Dust particles are quite rare compared to HI atoms, especially in such an early galaxy as the one I am studying. However, the dust particles exist, and a **lot** of photons are emitted, so an interaction between some Lyα photons and dust grains is inevitable. There are two possible outcomes of this. If our Lyα photon is the chosen one, it may simply scatter away, no harm done, and continue its journey throughout the galaxy. However, it might also get absorbed into the dust particle. Unlike absorption into an HI atom, this does not call for near-instant re-emission. The dust grain has consumed our photon and turned it into thermal energy, and it has died alone and forgotten by all. The dust grain will carry on with its life, unconcerned with being a cold-blooded murderer. Along the way it vibrates, absorbs other photons, and changes its properties. The dust will emit photons again, in the infrared spectrum - a ghastly mockery of the brave little Lyα photon it ate. Therefore we say that dust either scatters or destroys Lyα radiation.

As for our friendly little photon, I will let you make up your own ending. Did it escape? If so, as redshifted or blueshifted, or maybe it escaped during a short jump and was unaltered? Or did it meet its death, smashed flat towards the mountainside that is a dust particle? Go with the ending that makes you the most happy. But remember:

To a photon in such a galaxy is to be one amongst untold billions. It is to live in the most luminous and ionized gas imaginable. These are the tales of those galaxies. Forget the power of simulations and science, for so much is unresolved, never to be given enough computational power. Forget the promise of pristine gas and photon escape, for in the grim dark simulation there is only gas and dust. There is no direct escape amongst the stars, only an eternity of absorption and re-emission, and the laughter of thirsting supervisors[3].

2.6 Galactic Lyα Production

As seen in the Methods section, recombination Lyα luminosity can be calculated through $L = n_{\mathrm{e}} n_{\mathrm{HII}} V \alpha_{\mathrm{B}}(T)$, where the n_{e} and n_{HII} represents the number densities of electrons and ionized hydrogen respectively, V is the volume and $\alpha_{\mathrm{B}}(T)$ is the Case-B recombination coefficient. As luminosity is defined as total energy output per unit time, this can

[3]Loosely adapted from [19].

be used to see how much Lyα radiation each part of the galaxy produces. As we can see, there are four factors, and the production scales positively with all of them.

High number densities of electrons and ionized hydrogen HII simply means that this area there are a lot of electrons and ionized gas. This means we have a lot of the building blocks that is required for the recombination and subsequent Lyα emission to happen. This plays directly into a high $\alpha_{\mathrm{B}}(T)$; after all, having many building blocks would not matter if they did not recombine. High temperature means more energy to the gas, which causes the neutral HI atoms to split into HII and electrons in the first place. So all of these parameters are natural and intuitive inclusions in the Lyα photon production.

There are a few factors in the galaxy that affect the Lyα production. Three that I take into account in my model are **external ionization**, **internal ionization** and **self-shielding**. I have talked about the physical processes of ionization further up, but how do these affect the galaxy as a whole?

When I start working on the data, it "arrives ionized" to an extent. This is in part due to an external ionization, that is, ionization from outside the galaxy. In the model, this is presented as a uniform field. In reality, this comes from ultraviolet photons, creating this "background field". This affects the whole galaxy, except the self-shielded portions.

Next, we have ionization from internal feedback sources. The two I include and look at here are feedback from the active galactic nucleus (AGN) and from the stars in the galaxy.

The AGN is, to put it mildly, massively energetic. Therefore, one can assume that all gas within a certain distance of it will be fully ionized. For the stars, however, we must calculate. I will go more into the details of this in the "Methods" section, but the essence is that each star affects the gas around it to a certain degree. A big difference between the external and the internal ionization is that the internal does not take the self-shield into account, as it may originate from inside it.

This "self-shield" I have been talking about is a phenomenon that happens when a blob of unionised gas is hit by outside radiation. This "shield" forms around dense areas of gas, and prevents ionizing photons - mostly of the Lyman continuum variety - from penetrating and ionizing the gas behind it. Essentially, this means we will have pockets of unionised, neutral gas in between the ionized galaxy.

So where does this shield come from? Well, imagine you have a dense pocket of gas. Ionizing photons from surrounding stars and other sources will then hit this gas. Thus the outer layer will be ionized. So far so good. However, it will not stay ionized for long. Soon, this outer layer will start to recombine and de-excite. This de-excitation will, in approximately 68% of the cases, give Lyα radiation. Most of this radiation is not strong enough to ionize the inner layers of the pocket. This is especially true for the Lyα, as it carries an energy of $E_{\mathrm{Ly}\alpha} = 10.2\,\mathrm{eV}$, while the hydrogen gas requires an energy of $E_{\mathrm{ion}} = 13.6\,\mathrm{eV}$. So the re-emitted photons will not be energetic enough to ionize the gas inside the shield. Meanwhile, in emitting these photons, the hydrogen along the edge of shield will be neutral again, ready to absorb the next wave of incoming ionizing continuum photons.

So to put it like this: singular high-energy photon comes in, multiple low-energy photons go out. These will be unable to ionize the gas further, and will just scatter off the hydrogen particles. Thus, we will have neutral pockets within the large clouds of ionized gas.

All of this put together gives the model I am using for analysing the galaxy simulation.

Chapter 3

Methods

Here I describe the simulation and the analysis method.

The methods used are almost exclusively numerical. I have made use of the program *Pynbody* [20] to extract and analyse the simulation data.

3.1 The Ponos Simulation

The Ponos simulation is described in [21]. It is a high-resolution simulation, an alternative take on the run focusing on the halo originally dubbed "Ponos V". The high resolution version contains hydrodynamics and self-consistent baryonic physics. The version described in the paper has a higher resolution than the one I am analysing, but the physical processes are the same, and any properties I describe here are shared between the two simulation runs.

3.1.1 Smoothed Particle Hydrodynamics and Simulation Code

Smoothed particle hydrodynamics (SPH) is a computational method for simulation of fluids. It was developed by Gingold and Monaghan in 1977 [22]; and Lucy in 1977 [23]. Its main selling point is that it is gridless, letting us work on a particle-by-particle basis. This makes it easy to keep track of the physical properties of each particle in the fluid, and how they evolve over time.

The Ponos simulation was performed using the GASOLINE code [24]. It uses three kinds of matter particles in the simulation: stars, gas and dark matter.

GASOLINE models gas dynamics using SPH. Adding to the standard SPH formulation, it also includes a term for thermal energy and metal diffusion [24] [25]. The physical processes for galaxy formation include radiative cooling of gas, ionisation and heating from a uniform UV background [26]. The gas cools normally through radiation in the optically thin limit by solving the network of non-equilibrium reactions for HI, HII, HeI, HeII and HeIII.

An important point to note is that even when we go into high-resolutions, there will still be processes going on at sub-resolution levels that are important to the galaxy

evolution. Among these are the formation of stars and the impact of their feedback - in form of supernovae and stellar winds. These will both release energy and mass into nearby particles, but cannot be resolved. GASOLINE includes several sub-resolution models to deal with this feedback. The feedback sources are radiative cooling of gas, star formation and the above mentioned supernovae and stellar wind feedback. The supernovae inject energy into nearby particles, and the stellar wind will release additional mass into the system. The processes are based on [27].

For the supernova feedback, it is modelled such that each Type II supernova releases a thermal energy of 10^{51} erg into the surrounding gas, based on the maximum supernova blast range. This also temporarily turns off the cooling while the blast wave snowploughs through. For type Ia supernovae, the same energy is injected, but the cooling is not suspended. The supernovae also release mass into the surrounding gas, of $1.4\,\mathrm{M}_\odot$ per supernova. A fraction of this is also metals, meaning that the metallicity of the galaxy increases per supernova. Each supernova injects $0.63\,\mathrm{M}_\odot$ iron and $0.13\,\mathrm{M}_\odot$ oxygen into the surrounding gas.

The formation of supermassive black holes and an AGN are both not included in the simulation. This may play an important role in the energetic feedback and ionisation of the gas; as I discuss later.

3.1.2 Initial Conditions

The initial conditions (ICs) used are optimized for halo development until redshift $z = 6$. A ΛCDM model consistent with the results of the *Wilkinson Microwave Anisotropy Probe* 7 (WMAP7) is used. Parametrization is done by cosmological density fractions $\Omega_{m,0} = 0.272$, $\Omega_{\Lambda,0} = 0.728$ and $\Omega_{b,0} = 0.0455$. $\sigma_8 = 0.807$, $n_S = 0.961$ and $H_0 = 70.2$ km s^{-1} Mpc^{-1} [28] [29]. The halo is evolving in a box with size of 85.5 co-moving Megaparsec, and at $z = 0$ it reaches a mass of $m \sim 1.2 \times 10^{13}\mathrm{M}_\odot$.

The original initial conditions are part of the AGORA code-comparison project [30]. Ponos generates new initial conditions of the same halo by using the MUSIC code [31].

The run starts at $z = 100$, with a base cube of 128^3 particles per side.

3.1.3 Simulation Procedure

A five-step procedure is used to determine the high-resolution region on the initial conditions.

i) A 128^3 full-box simulation with only dark matter is being run to identify the main halo at $z = 6$.

ii) Particles within $2.5R_{vir}$ are traced back to the initial conditions.

iii) The local resolution of the ICs are increased. This is done by adding one level of refinement within a rectangular box containing all the back-traced particles.

iv) The ICs are evolved back to $z = 6$.

v) Step ii) is repeated, and two additional levels of refinement are added within the convex hull that contains all identified particles.

Each level of refinement increases the spatial resolution by a factor of 2 and the mass resolution by a factor of 8. Steps iv) and v) are iterated until 5 additional levels of refinement are added above the base level. At the last iteration, gas particles are introduced.

As for the particle masses, in the highest resolved areas the dark matter particles have a mass of $m_{\mathrm{DM}} = 35181.0\,\mathrm{M}_\odot$ and the gas has a mass of $m_{\mathrm{gas}} = 6831.24\,\mathrm{M}_\odot$.

For a more detailed description of Ponos, see [21].

3.1.4 Halo Finder

The Ponos simulation uses the **Amiga Halo Finder** (AHF) [32] [33] to detect dark matter halos. The finder defines a halo as a group of at least 100 particles bound within a virial radius.

3.2 Simulation analysis

3.2.1 Intrinsic Surface Brightness

tively) long time near the target atom. This will cause distortions in the bound electron's wave function, which may cause very complex quantum mechanical interactions. This becomes more and more prominent as n increases, and is mos To analyse the galaxy simulation, I have written my own code. The simulation snapshots are imported through *Pynbody* [3]. The goal is to find the luminosity and then surface brightness, which are described in equations 3.2 and 2.8 respectively.

I start off by importing some parameters directly from the simulation code, and use various equations to calculate the others I need. The vital imports are the mass of each particle m, its mass density ρ and its mass fractions f_i, where i is each particle species [1].

From the mass fractions, I find the number density of each particle species in each SPH particle through

$$n_i = \frac{f_i \rho}{m_i}, \tag{3.1}$$

where m_i is the mass of the particle species, a known, universal quantity.

The first step is to find the luminosity of the gas. To do that, I use equation 2.2 rewritten as

$$L = n_{\mathrm{HII}} n_{\mathrm{e}} V \alpha_{\mathrm{B,eff}}, \tag{3.2}$$

where V is the volume of the particle, N_{HII} is the number density of ionized hydrogen, N_{e} is the number density of free electrons and $\alpha_{\mathrm{B,eff}}$ is the effective Case-B

[1] When talking about "particle *species*" in this thesis I consistently refer to protons, electrons etc. When referring to "particles", I am talking about simulation particles, of which we have three types: gas, stars and dark matter. The "particles" in the simulation sense cover large areas of space; for example each "star particle" contains multiple stars.

recombination coefficient. This represents fraction of the Case-B recombination coefficient that produces results in Lyα emission.

The volume of the particle can be found simply by taking

$$V = \frac{\rho}{m} \tag{3.3}$$

for each particle, where ρ is each particle's mass density and m each particle's mass.

The effective recombination parameter is a bit trickier. This is done in two steps: first by using a fitting formula to find an approximate parameter, and then to find out how much of this turns into Lyα. Luckily for us, both of these have already been done.

As mentioned in the theory section, I assume the gas is opaque enough that $\alpha_{\rm B}$ is valid at all times.

The fitting formula we use is gathered from [34]. It goes as

$$\alpha_{\rm B}(T) = 2.753 \times 10^{-14} l_{\rm HI}^{1.5} (1 + (\frac{l_{\rm HI}}{2.740})^{0.407})^{-2.242}\,{\rm s}^{-1}\,{\rm cm}^{-2} \tag{3.4}$$

where $l_{\rm HI} = 2 \times 157807/T$ and T is the gas temperature.

To then find the fraction of this parameter that produces Lyα photons, we use

$$\alpha_{\rm B,eff} = P_{\rm B} \alpha_{\rm B} h\nu_0 \tag{3.5}$$

where ν_0 is the Lyα wave frequency and h is Planck's constant. $\alpha_{\rm B,eff}$ have the units of $\mathrm{erg\,cm^{-3}\,s^{-1}}$. As for P_B a fitting formula was introduced in [35] and is given as

$$P_{\rm B} = 0.686 - 0.106 \log(T \times 10^{-4}) - 0.009 \left(T \times 10^{-4}\right)^{-0.44}. \tag{3.6}$$

Now that we have these parameters for each particle, we can find a particle's luminosity by equation (3.2).

With this luminosity, I can plug my numbers into equation 2.8.

To do this, I instead project the data onto a 2D grid. As with launching photons and applying radiative transfer, I do this through MoCaLaTA [36].

3.2.2 Cooling Luminosity

The cooling - or collisional - luminosity of the galaxy can be found by equation 3.7. This goes like

$$L_{\rm Ly\alpha,cool} = h\nu_0 n_{\rm e} n_{\rm HI} q_{\rm 1s\to 2p}(T) V, \tag{3.7}$$

where $h\nu = 10.2\,{\rm eV}$ is the Lyα photon energy, $n_{\rm e}$ and $n_{\rm HI}$ are the number densities of electrons and neutral hydrogen; $q_{\rm 1s\to 2p}(T)$ is the collisional excitation rate coefficient (from now shortened to "q-factor") given by equation 3.8 [37], and V is the volume of the given particle or grid cell. For the q-factor,

$$q_{\rm 1s\to 2p}(T) = 2.41 \times 10^{-8} T_4^{-0.28} e^{-h\nu_0/k_{\rm B}T} {\rm cm^3 s^{-1}}, \tag{3.8}$$

where k_B is the Boltzmann constant. Multiplying these variables together is a simple process, that by all means should give a good, accurate collisional luminosity, but does not. See the "Results" and "Discussion" sections for more details.

3.2.3 Ionization

This is all well and good, but I want to make my model more realistic. To do this, I want improve the model's gas ionization.

An important factor to apply is the self-shielding. The way I do this is by declaring that within a certain limit, all gas is neutral. While this eliminates ionisation from external sources, it also invalidates sources within the shield. Thus, you miss out on some ionization that might be there otherwise, and my model becomes less precise.

The limits I examine are based on temperature and density. Generally, cold gas and dense gas means neutral gas. These are often synonymous, and are used as the basis for the shield I apply. Specifically, I investigate three definitions: a temperature-based shield where I neutralize anything colder than $T = 10^4\,\mathrm{K}$ (as this is the temperature where hydrogen starts ionizing); as well as a fine and a coarse density shield. What I mean by this is that the coarse shield will affect larger areas than the fine shield. The coarse shield is about neutralizing anything area where $n_\mathrm{H} > 0.01\,\mathrm{cm}^{-3}$, and the fine shield neutralizes any area where $n_\mathrm{H} > 0.1\,\mathrm{cm}^{-3}$.

The next step will be to include ionizations not present in the original simulation. There are two kinds we apply: ionization from stars and ionization from the AGN.

The method I use for the star ionization is very resolution dependent. This makes it an ill fit for the SPH, as the relatively small particles would be completely ionized using this method. Since I need the code to be in grid format to run MoCaLaTA anyway, this is an excellent time to convert my code from SPH in Python to a uniform grid in Fortran. The grid is $500 \times 500 \times 500$ cells long, with a physical size of $50 \times 50 \times 50$ kpc. The conversion is done numerically, by going through the position of each particle and finding out which grid cell each would be in. This size is chosen so that the resolution is reasonably high (being 100 pc per cell), as well as giving a neat temperature interpolation (see appendix). Then, depending on the parameter, I either divide by cell volume (to find ρ), or weigh it by mass (to find the other variables). This also gives me a great opportunity to calculate the star formation rate (SFR). For this, I look at the young stars in the simulation [2], and sum up the masses of these stars. This mass is then divided by $\mathrm{d}t = 35\,\mathrm{Myr}$ to find the SFR of each grid cell.

Figure 4.1 shows the complete simulation box, alongside an arbitrary zoomed in region and the box I choose to base my results on. As one can see, this is where the majority of the gas exists. It also goes just past the virial radius, which means we get the entire "significant" portion of the galaxy within the box limits.

[2] Defined as the stars where $\mathrm{age}_\mathrm{Universe} - \mathrm{time}_\mathrm{formation} < (\mathrm{d}t = 35\,\mathrm{Myr})$

Star Ionization

Once we have the code in grid format, I apply the star ionization, using equations 3.9 and 3.10. The basis of the method lies in calculating a part ΔX_{HI} to subtract from the number fraction neutral hydrogen. This can be converted to a mass fraction through

$$\Delta f_{\mathrm{HI}} = \Delta X_{\mathrm{HI}} \sum_i \frac{n_i m_{\mathrm{HI}}}{n_i m_i}, \tag{3.9}$$

where f is mass fraction, X is number fraction, i loops over particle species, n is cell number density and m is particle species mass.

I calculate the fraction of ionized hydrogen through $f_{\mathrm{HII}} = 0.764 - f_{\mathrm{HI}}$, where 0.764 is a globally set mass fraction of hydrogen atoms in the simulation. This will in turn give me the fraction of the ionized HII. With this fraction, I can use equation (3.2) again to find the new, stellarly ionized Lyα luminosity. The formula for finding ΔX_{HI} is given as [10]

$$\Delta X_{\mathrm{HI}} = \frac{Q_{\mathrm{ion}} m_{\mathrm{ion}}}{n_{\mathrm{HI}}^2 \alpha_{\mathrm{B}}(T) V_{\mathrm{cell}}}. \tag{3.10}$$

Here X_{HI} is the number fraction of neutral hydrogen; α_{B} is the recombination coefficient and V_{cell} is the cell volume. The other two are a bit less general: $Q_{\mathrm{ion}} = 2 \times 10^{53} \frac{\mathrm{SFR}}{1\,\mathrm{M}_\odot\,\mathrm{yr}}$ is to factor in the star formation rate (SFR). In [38] it is shown that this works for a range of different stellar models. m_{ion} can be seen as the number fraction of fully ionized Strömgen spheres in a neutral cell. I choose to have it as 1 for this project. $\alpha_{\mathrm{B}}(T)$ is the case-B hydrogen recombination parameter, and n_{HI} is the number density of neutral hydrogen.

This number fraction is then converted into the equivalent mass fraction, through equation (3.9). In this case that is HI, HII, HeI, HeII, and HeIII. Then, Δf_{HI} is subtracted from the existing f_{HI}, to get a new value. This new value is used to calculate the post-stellar ionization luminosity in the given grid cell.

AGN Ionization

As for the AGN ionization, the method is very crude, but should be appropriate enough. I simply choose a radius from the center and declare that everything within this radius is fully ionized. As discussed in the aptly named "Discussion" sections, it turns out the star ionization is so strong that the AGN ionization has a minimal effect in comparison. Thus I set the AGN to have a radius of 1 kpc.

As I see it, there are three inherent weaknesses in this approach. The first is that the size of the AGN is more or less guesswork. The second is that I do not take any jets into account, and assume the AGN is completely spherical. The third is that this is a binary set-up; either everything is affected by the AGN or nothing is. There is no transition. With this in mind, I proceed to the radiative transfer itself.

3.2.4 Lyα Radiative Transfer

The Lyα radiative transfer is done with a code called MoCaLaTA, written by my co-supervisor Peter Laursen [36]. MoCaLaTA is a grid-based code, that performs radiative transfer of Lyα radiation in a simulated galaxy. The process starts by finding luminous cells. The more luminous a cell it, the higher chance it has of emitting a photon package. Once the emitting cells have been found, MoCaLaTA will emit a photon in a random direction. The code will integrate the optical depth τ along the line of the emitted photon. A scattering will happen after a distance

$$d = \frac{\tau}{n_{\rm HI}\sigma_{\rm HI} + n_{\rm dust}\sigma_{\rm dust}}, \tag{3.11}$$

where d is the distance, τ is the optical depth, $n_{\rm HI}$ and $n_{\rm dust}$ are the number densities of HI gas and dust; and $\sigma_{\rm HI}$ and $\sigma_{\rm dust}$ are the cross-sections of HI gas and dust. $n_{\rm HI} \gg n_{\rm dust}$, so the vast majority of the scatterings will be off the hydrogen atoms. n and σ are cell-dependent variables (σ depends on temperature), and are uniform within each cell. A random value of τ is determined from a probability distribution of $P(\tau) = e^{-\tau}$. From this value of τ we can then calculate the distance as in equation 3.11[3] .

As described in the theory section, the by far most likely collision is with a neutral hydrogen atom. If this happens, a weighted random new direction will be assigned to the photon, and the next turn will begin. This will continue until the photon either escapes the galaxy or is destroyed by a dust particle.

The amount of "photons" emitted is dictated by the user. In this project I emit $N_\gamma = 100000$ photons, which mean I divide the original luminosity by 100000 and send out that many packages, each holding a fraction of the original luminosity. Thus each photon package represents $\frac{L}{E_\gamma N_\gamma}$ photons, where L is the galaxy's total luminosity and E_γ is the energy of a single photon.

The dust type I run MoCaLaTA with is "Small Magellanic Cloud (SMC) dust". At the wavelength of Lyα photons, the albedo is $A \approx 0.32$. This means for each dust collision the photon has a 32% chance of scattering, and a 68% chance of being destroyed. The code handles destruction simply by ending the photon's journey right there and then, and moving on to the next photon without recording an escape.

MoCaLaTA makes a cube around the galaxy, which can be thought of as a six-sided die. Each side of the die corresponds to a window from which one can look at the galaxy - dubbed xm, xp, ym, yp, zm and zp, for "x minus", "x plus" and so on. Looking in

[3] A physically inaccurate, but intuitive way to think about it is of τ as the "movement speed" of the photon, as if the photon was a character in a turn-based video game. Each turn starts by rolling a die, thus assigning a movement speed τ to the particle for this turn. The turn ends when the particle has used up all its movement speed. However, some of the "terrain", represented by the density n, is more difficult to cross than others. Thus, in some cells the character uses more of his movement resource to move the same distance than he would in other cells - as if he crossed a plain and then went into a dense forest covered in underbrush. So the higher the density, the more of the movement resource is used up per step the character takes. When he has zero movement left, our character - the photon - will stop, and the turn will go into the scattering phase. In this way, the density and temperature (through σ) will determine how often the photon scatters, as well as the random factor of the optical depth.

through the xm window means looking along the positive direction - from the negative, thus "xm" - of the x-axis, with the window being spanned by the y- and z-axes.

This window we look through has a third dimension as well, stretching outwards towards us. On the axis of this dimension we find wavelength. Drawing a line along this axis and into the simulation box, we count the amount of scatterings that happen behind the corresponding pixel of the line. For each scattering, we look at the wavelength of this particular photon, and add a value $P_{\phi,\theta}e^{-\tau}$ to the corresponding wavelength. $P_{\phi,\theta}$ is the probability of being scattered in a given direction, τ is the optical depth between the scattering point and the edge of the box.

This will give us six cubes, each attached to the galaxy die, with x-y-axes spanning the area of the cube side and the z axis going outwards. I set the resolution to be $200 \times 200 \times 300$. The way to use these are through collapsing. If we collapse this cube along the z-axis, we get all the scatterings in each pixel added up, and can use this to find the surface brightness. If we collapse along the x and y axis, however, we get the wavelengths of every pixel. This is shown in figures 4.6 through 4.11, with the rightmost subplots showing the surface brightness, and the rightmost ones the wavelength spectrum.

Chapter 4

Results

Here I will first present the results of my research.

4.1 Simulation Properties

Here I will present some of the properties of the simulation.

The original simulation size is a $85.5 \times 85.5 \times 85.5\,\text{comoving}\,\text{Mpc}^3$ box, with gas stretching 388.1 kpc, 546.6 kpc and 424.7 kpc in the x, y and z directions respectively. However, the virial radius is only 21.97 kpc. As figure 4.1 shows, much of the simulation is just empty space. Therefore, I choose to zoom in on a box with dimensions 50kpc $\times$ 50kpc $\times$ 50kpc around the center of the largest galaxy. This is a neat, rounded number that covers the entire virial radius.

The physical properties of the gas within this simulation are presented in table 4.1. I present the minimum, maximum and means of the variables, as well as the sum where it makes sense.

Figure 4.2 shows some general properties of the simulation, both a full view and one zoomed in box. The density figures reveals that the main galaxy is in the middle of a galaxy merger. This is an explanation as for why the star formation rate and luminosity have so unusually high values. The temperature maps show that the temperature gets quite high, possibly due to supernova feedback.

Star Formation

Using the interpolation method described in section 3.2.3. This gives a star formation rate (SFR) of $41.42\,\text{M}_\odot\,\text{yr}^{-1}$. This is a high SFR for galaxies of this redshift - it seems the Ponos galaxy is very star-forming. This is supported by figure 4.3, which shows the fraction of star mass versus the total halo mass of the galaxy. As we can see, the Ponos galaxy is quite above the normal at all redshifts. Figure 4.4 shows that this formation rate went up exponentially the 150 million years, possibly as a result of the ongoing merger event seen in figure 4.2. At the current redshift, $z = 6.5$, it is at an all-time high.

Table 4.1: Parameters of the particles in the zoomed-in $50 \times 50 \times 50\,\mathrm{kpc}^3$ simulation box.

Component	Parameter	Minimum	Maximum	Mean	Sum	Units
Gas	Luminosity, rec	0.00	7.52×10^{39}	2.44×10^{37}	6.25×10^{43}	erg s^{-1}
	Luminosity, cool	0.00	5.58×10^{41}	8.27×10^{38}	2.11×10^{45}	erg s^{-1}
	Mass	6.15×10^{3}	2.92×10^{4}	7.52×10^{3}	1.92×10^{10}	$M_\odot$
	Temperature	113.68	4.32×10^{7}	2.34×10^{5}	-	K
	ρ	5.18×10^{-29}	1.68×10^{-21}	9.04×10^{-23}	-	g cm^{-3}
	n_{HI}	2.54×10^{-13}	767.64	29.37	-	cm^{-3}
	n_{HII}	0.00	747.73	11.90	-	cm^{-3}
	n_{e}	0.00	862.84	13.92	-	cm^{-3}
	n_{tot}	5.29×10^{-5}	1672.85	58.26	-	cm^{-3}
	f_{HI}	1.00×10^{-12}	0.764	0.33	-	-
	f_{HII}	0.00	0.764	0.44	-	-
Stars	Mass	4.73×10^{3}	6.83×10^{3}	5.65×10^{3}	5.13×10^{9}	$M_\odot$
	Formation time	141.24	865.78	726.53	-	Myr
Dark matter	Mass	3.52×10^{4}	3.52×10^{4}	3.52×10^{4}	8.99×10^{10}	$M_\odot$
Total	Mass	-	-	-	1.14×10^{11}	$M_\odot$

Table 4.2: General parameters of the simulation; as well as component masses. Here I present first those within the virial radius, then for the whole simulation, then, for completeness' sake, a repeat of the masses within the $50 \times 50 \times 50\,\mathrm{kpc}^3$ box from table 4.1.

Property	Value	Unit
Star formation rate	41.42	$M_\odot$/yr
Virial radius	21.97	kpc
Virial mass	1.24×10^{11}	$M_\odot$
Gas mass (vir)	1.65×10^{10}	$M_\odot$
Stellar mass (vir)	4.99×10^{9}	$M_\odot$
Dark matter mass (vir)	1.02×10^{11}	$M_\odot$
Simulation size	1.14×10^{4}	kpc
Simulation mass	2.32×10^{16}	$M_\odot$
Gas mass (sim)	4.38×10^{10}	$M_\odot$
Stellar mass (sim)	5.13×10^{9}	$M_\odot$
Dark matter mass (sim)	2.32×10^{16}	$M_\odot$
Box size	50	kpc
Box mass	1.14×10^{11}	$M_\odot$
Gas mass (box)	1.92×10^{10}	$M_\odot$
Stellar mass (box)	5.13×10^{9}	$M_\odot$
Dark matter mass (box)	8.99×10^{10}	$M_\odot$

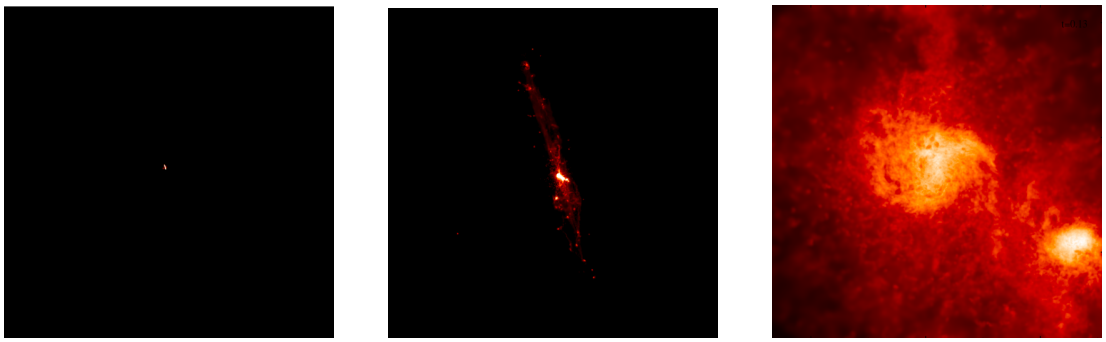

(a) Full simulation box.

(b) Arbitrarily zoomed in simulation box.

(c) Simulation box zoomed in to $25 \times 25 \times 25\,\mathrm{kpc}$

Figure 4.1: Visual image of the simulation box, represented by the logarithmic column density $\log(\rho_{\mathrm{col}})$. Visualizes how much of the box is empty space, and why zooming in on the gas is purposeful. Made with SPLASH [3].

4.2 Intrinsic Lyα Luminosity

Using the method described in section 3.2.1, and particularly equation 3.2, I get a recombination Lyα luminosity of $L = 3.07 \times 10^{44}\,\mathrm{erg\,s^{-1}}$. This is a bit on the high end, and the result of it *only* being affected by the background radiation. In order to make the model more realistic, self-shielding and ionization are applied.

The first big choice comes when deciding what self-shielding method to use. I have here tried four different models, as presented in section 3.2.3. They all give a total luminosity, and a cut-off luminosity in the zoomed in box I choose to further examine. Figure 4.5 is an invaluable tool for determining which areas to neutralize, so to speak. The results of each self-shielding model are presented in table 4.3.

Table 4.3: How the various methods of self-shielding affect the galaxy's recombination Lyα luminosity.

Shield	Simulation luminosity		Box luminosity	
None	L	$= 3.07 \times 10^{44}\mathrm{erg\,s^{-1}}$	L	$= 3.05 \times 10^{44}\mathrm{erg\,s^{-1}}$
$n_{\mathrm{H}} > 0.1\,\mathrm{cm^{-3}}$	$L_{N>0.1}$	$= 9.14 \times 10^{41}\mathrm{erg\,s^{-1}}$	$L_{N>0.1}$	$= 3.14 \times 10^{41}\mathrm{erg\,s^{-1}}$
$n_{\mathrm{H}} > 0.01\,\mathrm{cm^{-3}}$	$L_{N>0.01}$	$= 7.72 \times 10^{40}\mathrm{erg\,s^{-1}}$	$L_{N>0.01}$	$= 8.75 \times 10^{39}\mathrm{erg\,s^{-1}}$
$T < 10^4\,\mathrm{K}$	$L_{T<10^4}$	$= 6.36 \times 10^{43}\mathrm{erg\,s^{-1}}$	$L_{T<10^4}$	$= 6.25 \times 10^{43}\mathrm{erg\,s^{-1}}$
$n_{\mathrm{H}} > 0.1\,\mathrm{cm^{-3}}$ & $T < 10^4\,\mathrm{K}$	L	$= 6.36 \times 10^{43}\mathrm{erg\,s^{-1}}$	L	$= 6.25 \times 10^{43}\mathrm{erg\,s^{-1}}$

First off, there are two density shields. In the first I declare that all particles with a hydrogen density of $n_{\mathrm{H}} > 0.1\,\mathrm{cm^{-3}}$ are fully neutral. This gives a total simulation Lyα luminosity of $L_{n>0.1} = 9.14 \times 10^{41}\,\mathrm{erg\,s^{-1}}$. The luminosity in the box is $L_{n>0.1} = 3.14 \times 10^{41}\,\mathrm{erg\,s^{-1}}$.

For the coarser density shield I set that all particles with $n_{\mathrm{H}} > 0.01\,\mathrm{cm^{-3}}$ are fully

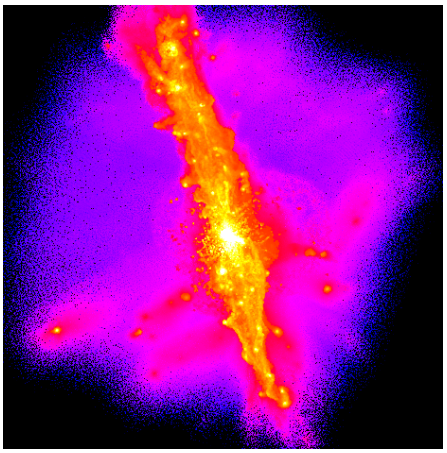

(a) Logarithmic gas density $\log(\rho)$ of a $178 \times 178 \times 178\,\mathrm{kpc}^3$ box for values $4 \times 10^{-30}\,\mathrm{g\,cm^{-3}}$ to $4 \times 10^{-23}\,\mathrm{g\,cm^{-3}}$.

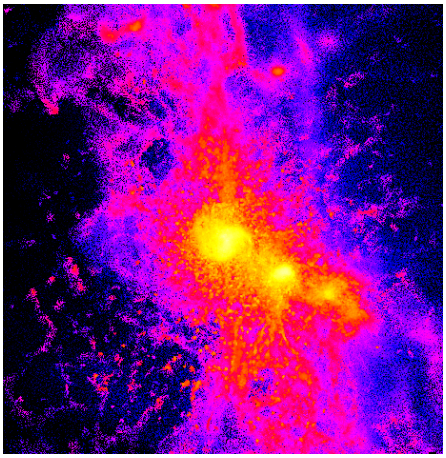

(b) Logarithmic gas density $\log(\rho)$ of a zoomed in box of $50 \times 50 \times 50\,\mathrm{kpc}^3$ for values $4 \times 10^{-27}\,\mathrm{g\,cm^{-3}}$ to $4 \times 10^{-21}\,\mathrm{g\,cm^{-3}}$.

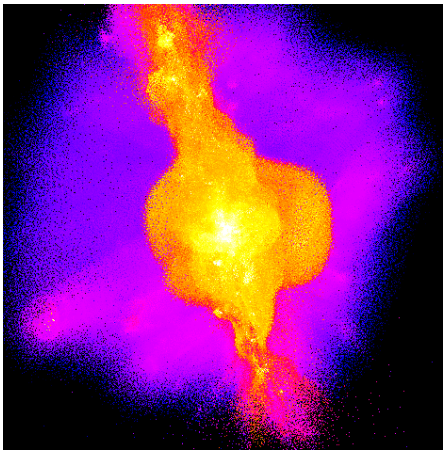

(c) Logarithmic gas temperature $\log(T)$ of a $178 \times 178 \times 178\,\mathrm{kpc}^3$ box for values $1 \times 10^3\,\mathrm{K}$ to $1 \times 10^7\,\mathrm{K}$.

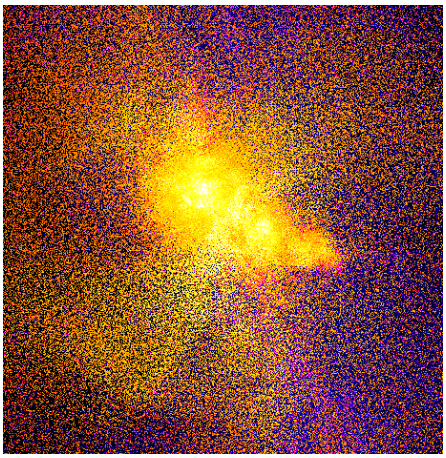

(d) Logarithmic gas temperature $\log(T)$ of a zoomed in box of $50 \times 50 \times 50\,\mathrm{kpc}^3$ for values $1 \times 10^4\,\mathrm{K}$ to $1 \times 10^7\,\mathrm{K}$.

Figure 4.2: Temperature T and mass density ρ of the gas, for the whole galaxy and for the zoomed box. Both values and colour scales are logarithmic, with black meaning cold and yellow meaning warm. Made using the Tipsy visualization tool from N-Body Shop (`http://faculty.washington.edu/trq/hpcc/`).

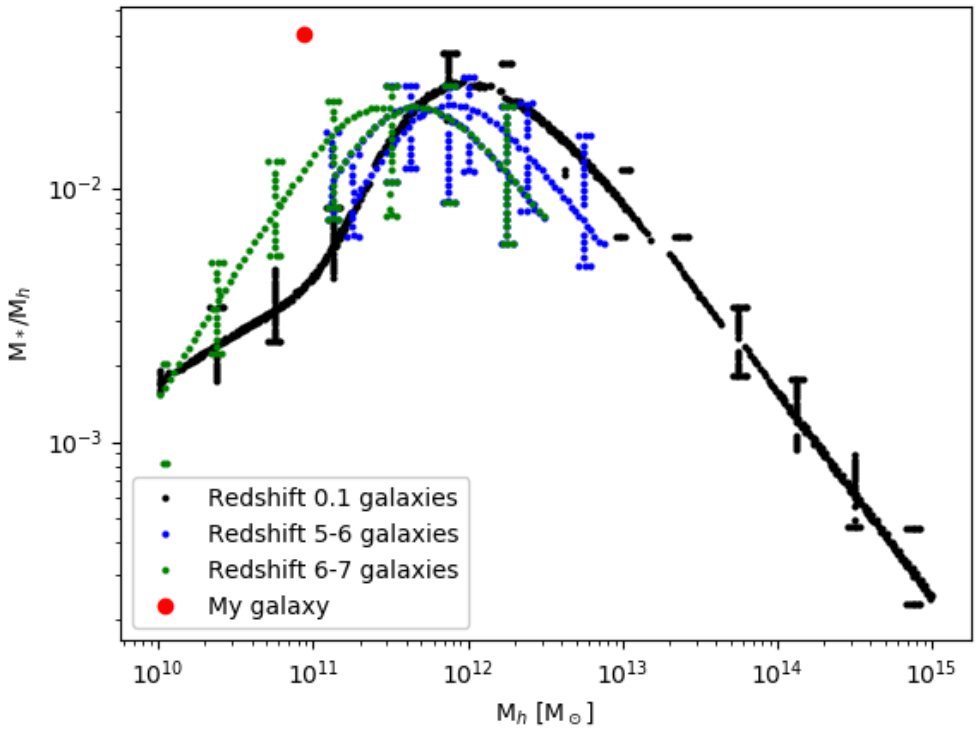

Figure 4.3: Star mass percent as a function of total halo mass. The Ponos galaxy has a higher percentage of stars than normal, as seen in other data that deems it a galaxy with high star formation. Observational data from [4].

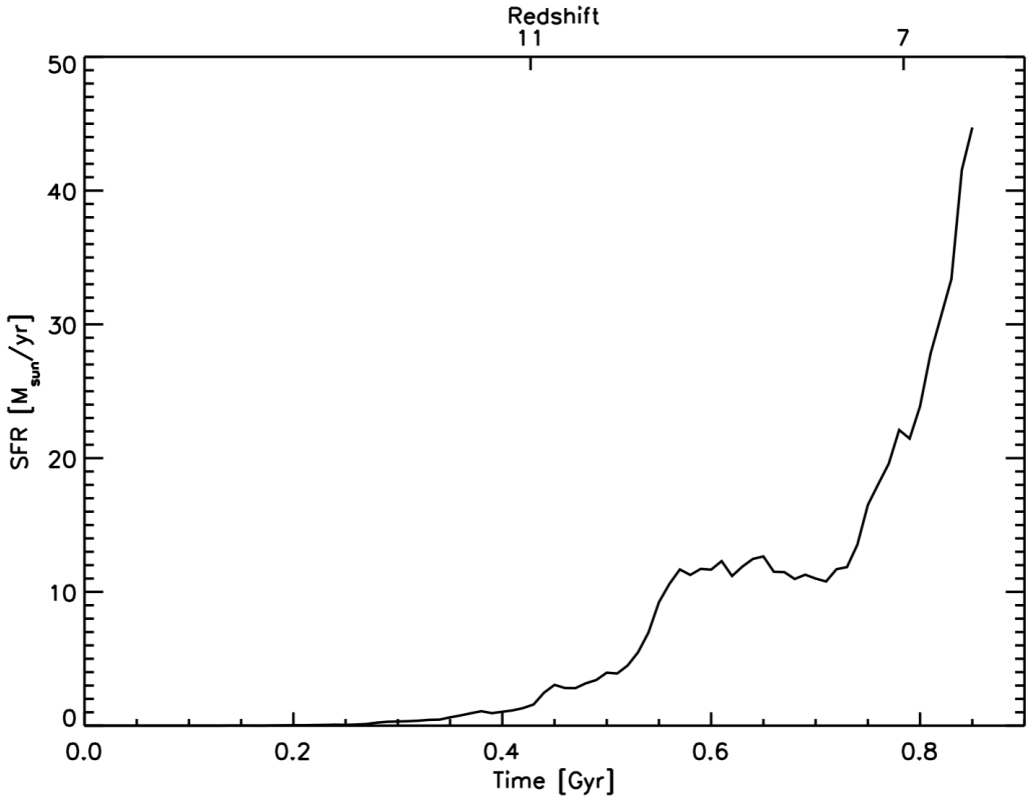

Figure 4.4: Star formation history of the galaxy. Figure made using a routine by Sijing Shen.

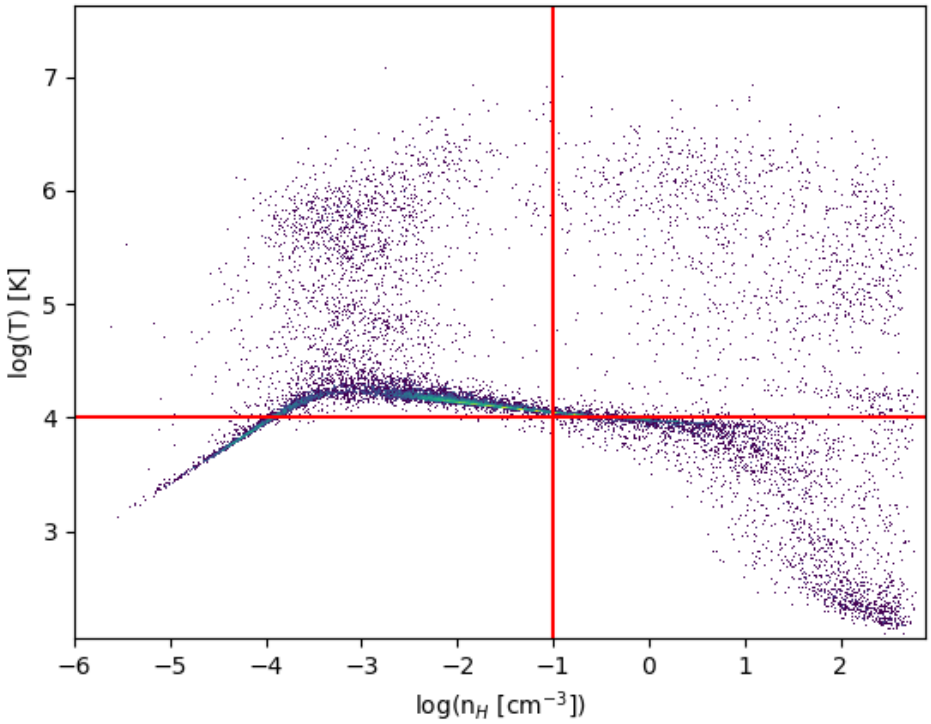

Figure 4.5: Logarithmic distribution of temperature as a function of hydrogen number density. Markers show the zones the self-shielding schemes of temperature and the fine density shield would affect. Neutralization line for $n_{\mathrm{H}} > 0.01\mathrm{cm}^{-3}$ not provided, as this model is quickly discarded.

neutral. This gives $L_{N>0.01} = 7.72 \times 10^{40}\,\mathrm{erg\,s^{-1}}$ before zooming in on the box and $L_{n>0.01} = 8.75 \times 10^{39}\,\mathrm{erg\,s^{-1}}$ after. This model is quickly disregarded, as it neutralized an unreasonably large part of the galaxy.

For the temperature cut-off, I look at the cold areas, and declare them to be neutral. This is in itself a bit unconventional, as self-shielding is a density-based method. However, as the upper right quadrant of figure 4.5 shows, the vast majority of the dense gas is hotter than $10^4\,\mathrm{K}$. Thus neutralizing it would be very non-physical, and using a temperature-based shield would be the lesser of two evils. The temperature limit I choose is $T = 10^4\,\mathrm{K}$, as this is the temperature at which hydrogen has enough energy to start ionizing. With this method, I get a total luminosity of $L_{T<10^4} = 6.36 \times 10^{43}\,\mathrm{erg\,s^{-1}}$ before the cut-off and $L_{T<10^4} = 6.25 \times 10^{43}\,\mathrm{erg\,s^{-1}}$ after.

The fourth model combines the first and third. In this model I only neutralize the lower quadrant of figure 4.5; that is, where $n_{\mathrm{H}} > 0.1\,\mathrm{cm}^{-3}$ **and** $T < 10^4\,\mathrm{K}$. This model gives me essentially the same results as the temperature shield. However, I feel it is the most physically accurate model of the four, and proceed to use this one.

The results are summed up in table 4.3.

Figure 5.1 shows the ionization as a function of temperature. As seen in the figure $T = 10^4\,\mathrm{K}$ is a decent approximation, as it is within this range the ionization starts happening.

Cooling Luminosity

As per equation 3.7, the Lyα cooling luminosity should be a function of the electron and HI number densities n_e and n_HI, the collisional excitation rate coefficient (q-factor) $q_{1\mathrm{s}\to 2\mathrm{p}}(T)$ and the volume V. It should also be a few percentages of the Lyα recombination luminosity. This, however, turns out to not be the case. Instead, we get $L_{\mathrm{cool,Ly}\alpha} = 2.11 \times 10^{45}$; whereas the intrinsic $L_{\mathrm{rec,Ly}\alpha} = 6.25 \times 10^{43}$. Therefore I choose to not include it in the project, other than as an unsolved curiosity. See the "Discussion" section for an examination of relevant figures 5.1, 5.2 and 5.3.

4.3 Ionization Approximations

After interpolating the variables to a grid, they remain in a mostly recognizable form. See the appendix for histograms showing the difference between the SPH and the interpolated grid. One important result form the interpolation is that after using equation 3.2 to calculate the new Lyα luminosity, the result is $L_{\mathrm{rec,Ly}\alpha\mathrm{,grid}} = 1.60 \times 10^{43}\,\mathrm{ergs}^{-1}$. As we can see, this is a significant difference from the particle code. However, I proceed, and apply AGN and star ionization as described in the "methods" section. After applying an AGN with radius 1 kpc, I get $L_{\mathrm{rec,Ly}\alpha\mathrm{,grid,AGN}} = 1.60 \times 10^{43}\,\mathrm{ergs}^{-1}$. Looking further into the digits, applying this AGN gives an increase of 0.0013% - a very insignificant number. After then doing star ionization, the luminosity is up to $L_{\mathrm{rec,Ly}\alpha\mathrm{,grid,AGN,stars}} = 7.68 \times 10^{43}\,\mathrm{ergs}^{-1}$.

Table 4.4 shows how luminosity and number of ionized cells differ based on how large the AGN radius is. To get even a somewhat significant increase, the AGN must have an ionization radius of almost half the virial radius. Since this is unrealistic, I will, for simplicity's sake, use the data from where $R_\mathrm{AGN} = 1\,\mathrm{kpc}$.

Another thing table 4.4 shows is how the ionization schemes affect the cells. As we can see, not a huge number of cells have been affected. However, by cross-referencing with figure 4.5 one can assume that the densest and most central cells have been. These are the ones that are responsible for the majority of the Lyα production. So even if so few cells are affected by the extra ionization, we still increase the luminosity by a factor of 7.

4.4 Surface Brightness

For finding the surface brightness I used the code MoCaLaTA, written by Peter Laursen [36]. I sent out $n_\gamma = 10^5$ photon packets, and let them scatter off dust in the galaxy. I also did the same without scattering as to being able to compare the intrinsic and the

Table 4.4: Luminosity changes with different AGN radii. The first row shows the luminosity after only the AGN ionization has been applied, the second after AGN and then star ionization. The virial radius is $R_{\text{vir}} = 21.97\,\text{kpc}$. I also show the amount of particles that are unaffected, partly ionized and fully ionized by the post-processing of the simulation. The total number does not match up to the $500 \times 500 \times 500$ grid due to the fact that the empty cells have been disregarded.

AGN radius:	1 kpc	5 kpc	10 kpc	R_{vir}
$L_{\text{a/AGN}}\,[\,\text{erg}\,\text{s}^{-1}]$	1.596528×10^{43}	1.596878×10^{43}	1.920463×10^{43}	1.518833×10^{44}
$L_{\text{a/stars}}\,[\,\text{erg}\,\text{s}^{-1}]$	7.687970×10^{43}	7.688321×10^{43}	7.993162×10^{43}	1.518833×10^{44}
Unaffected	1.20×10^{6}	1.18×10^{6}	1.03×10^{6}	3.63×10^{5}
Partly ionized	2.58×10^{3}	2.58×10^{3}	2.40×10^{3}	0
Fully ionized	2.30×10^{4}	4.81×10^{4}	1.96×10^{5}	8.67×10^{5}

scattered surface brightnesses. MoCaLaTA offers views of the luminosity and surface brightness from all directions in the galaxy cube grid. One can think of it as a die, with each side corresponding to a positive and negative x, y and z-direction.

The three main results from this are the surface brightness map, and the surface brightness profile, and the spectrum. The surface brightness maps and spectra for each direction and appropriate spectra are shown in figures 4.6 through 4.11. They have been made on 200×200 pixel grids, each with a physical length of $50 \times 50\,\text{kpc}^2$. The effects of the Ly$\alpha$ scattering is clearly visible. Each of the six directions correspond to looking in from the positive or negative x, y, and z-direction, labelled "xm", "xp", "ym", "yp", "zm" and "zp".

Figures 4.12 through 4.14 show the surface brightness profiles. These have been shifted so that they start on the brightest pixel in the scattered image. This is to make it easier to compare with observations; when observing it is the scattered image we see, and we typically define the brightest visible point as being the center. Table 4.5 shows the flux and escape fraction in each direction, as well as the most luminous pixel and its distance from the galactic center. The escape fraction is done by dividing the sum of the integral field unit IFU by the number of emitted photons N_γ.

Figure 4.15 shows the surface brightness profiles in comparison to observations. Subfigure 4.15a shows compared to galaxies at similar redshifts ($5 < z < 6$) presented in [5]. As we can see, the Ponos galaxy is orders of magnitude more luminous than these galaxies. Based on this, and the SMHM chart in figure 4.3, the Ponos galaxy seem to be superluminous. Therefore, I compare with the galaxies presented in [10]. As these are giant Lyα nebulae, their profiles extend much further out than mine. Therefore I compare in the overlapping areas. Based on subfigure 4.15b, there seem to be a good match with the superluminous Lyα nebulae.

The spectra shown in figures 4.6 through 4.11 shows peaks at red- and blueshift. This is expected, as the Doppler shifted photons travel longer distances uninterrupted, and are therefore more prone to escape. We also have high escape towards the central

line $\lambda = 1216$ Å. This likely comes from the outer parts of the galaxy, where the gas is not dense enough to stop the non-shifted photons from escaping. For the intrinsic spectra, the lines is centred neatly around 1216 Å, as expected.

Table 4.5: Lyα flux in each direction, as well as most luminous pixel and its distance from the galactic center. For the surface brightness profiles in figures 4.12 through 4.14, the brightest pixels of the scattered Lyα photons are used. The directional axes are tilted such that the origin will always be in the lower left corner.

Direction	Flux $[\mathrm{erg\,s^{-1}\,cm^{-2}}]$	Esc. fraction	Brightest pixel [kpc]	Distance from center
xm, scatter	2.59×10^{-18}	0.70	(110 z, 108 y)	3.20
xp, scatter	3.20×10^{-18}	0.78	(107 y, 102 z)	1.82
ym, scatter	1.08×10^{-18}	0.33	(108 x, 119 z)	5.15
yp, scatter	2.61×10^{-18}	0.68	(110 z, 108 x)	3.20
zm, scatter	4.22×10^{-18}	0.91	(119 y, 102 x)	4.78
zp, scatter	3.00×10^{-18}	0.80	(101 x, 118 y)	4.51
xm, intrinsic	6.94×10^{-18}	0.97	(102 z, 108 y)	2.06
xp, intrinsic	6.87×10^{-18}	0.98	(108 y, 102 z)	2.06
ym, intrinsic	5.72×10^{-18}	0.97	(108 x, 119 z)	5.15
yp, intrinsic	6.72×10^{-18}	0.97	(119 z, 108 x)	5.15
zm, intrinsic	5.42×10^{-18}	0.99	(119 y, 102 x)	4.78
zp, intrinsic	5.47×10^{-18}	0.99	(102 x, 119 y)	4.78

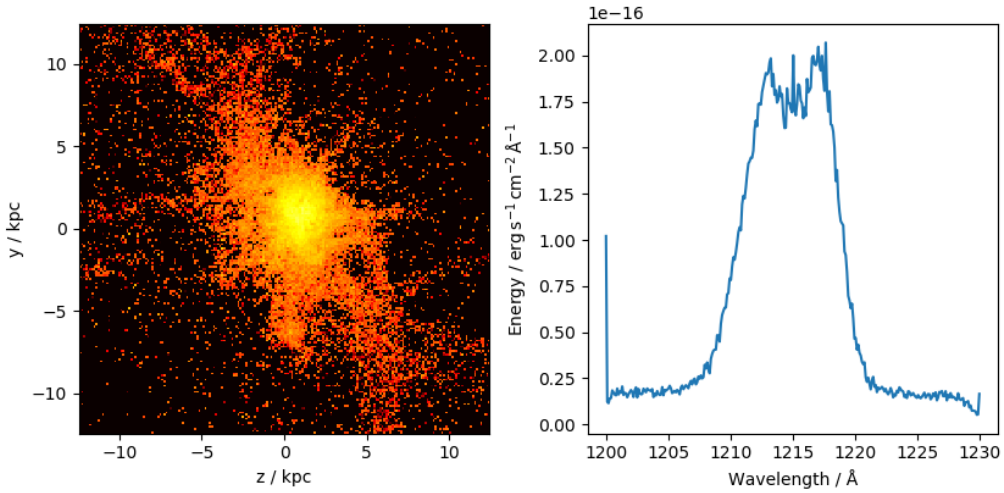

(a) Scattered Lyα surface brightness map and spectrum in negative x-direction.

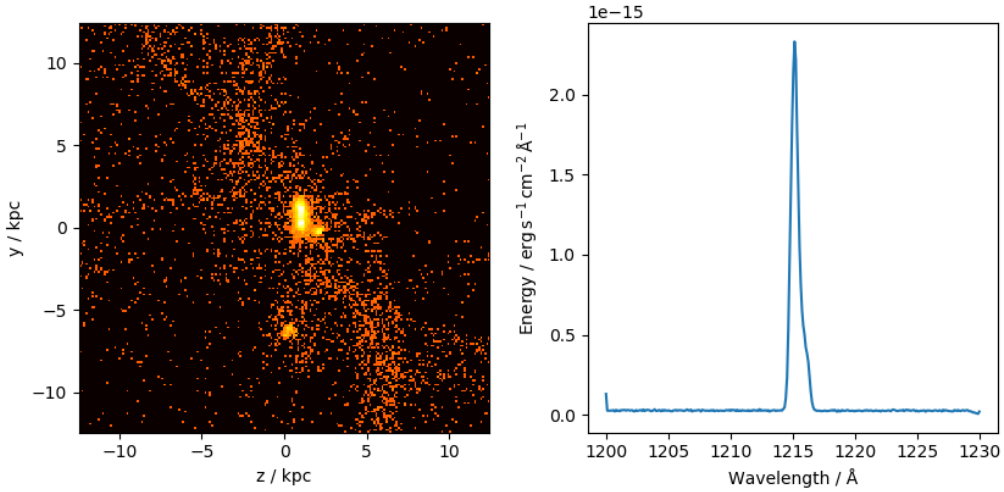

(b) Intrinsic Lyα surface brightness map and spectrum in negative x-direction.

Figure 4.6: Lyα surface brightness maps and spectra in the xm-direction. Shows the effect of Lyα photon scattering. The map covers surface brightnesses in the range $10^{-22} - 10^{-14}\,\mathrm{erg\,s\,cm^{-2}\,arcsec^{-2}}$.

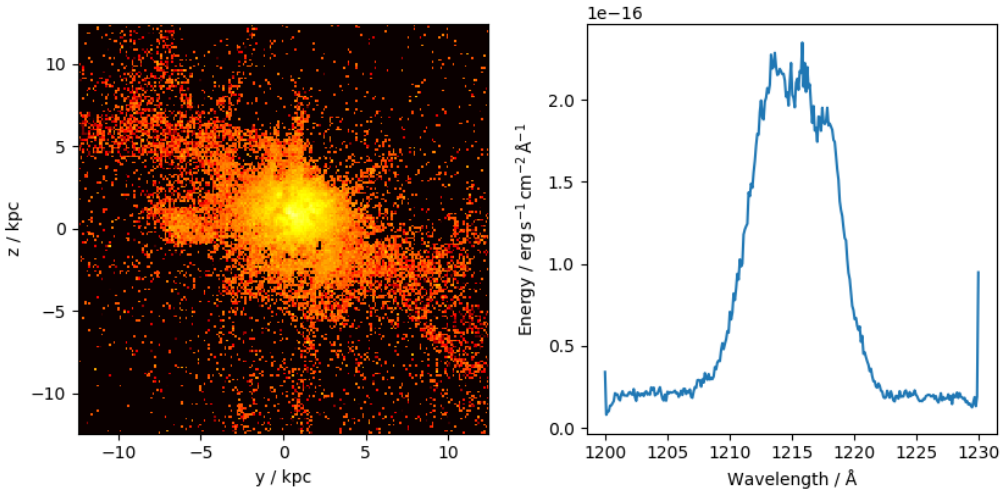

(a) Scattered Lyα surface brightness map and spectrum in positive x-direction.

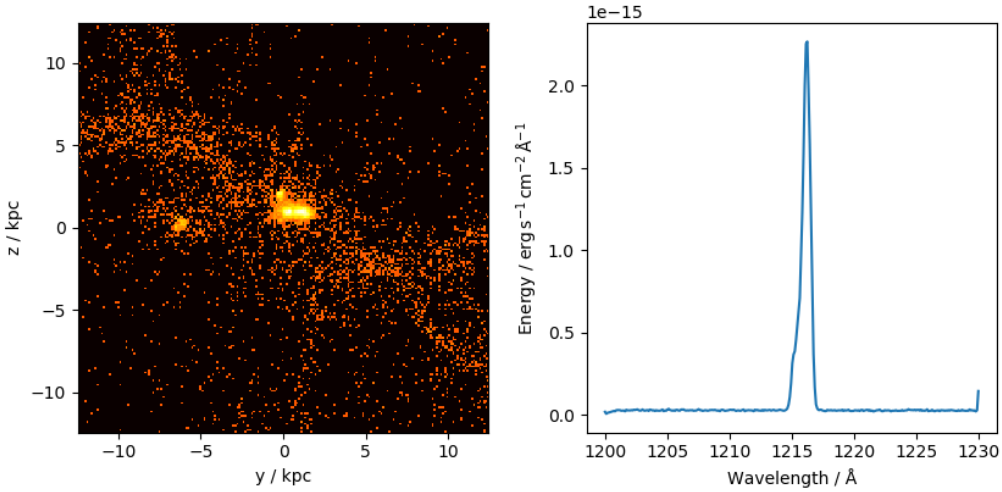

(b) Intrinsic Lyα surface brightness map and spectrum in positive x-direction.

Figure 4.7: Lyα surface brightness maps and spectra in the xp-direction. Shows the effect of Lyα photon scattering. The map covers surface brightnesses in the range $10^{-22} - 10^{-14}\,\mathrm{erg\,s\,cm^{-2}\,arcsec^{-2}}$.

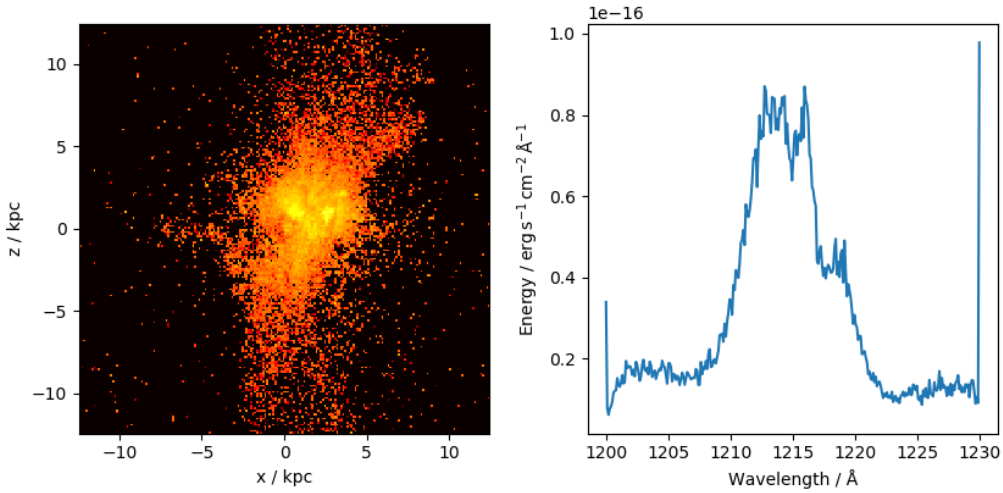

(a) Scattered Lyα surface brightness map and spectrum in negative y-direction.

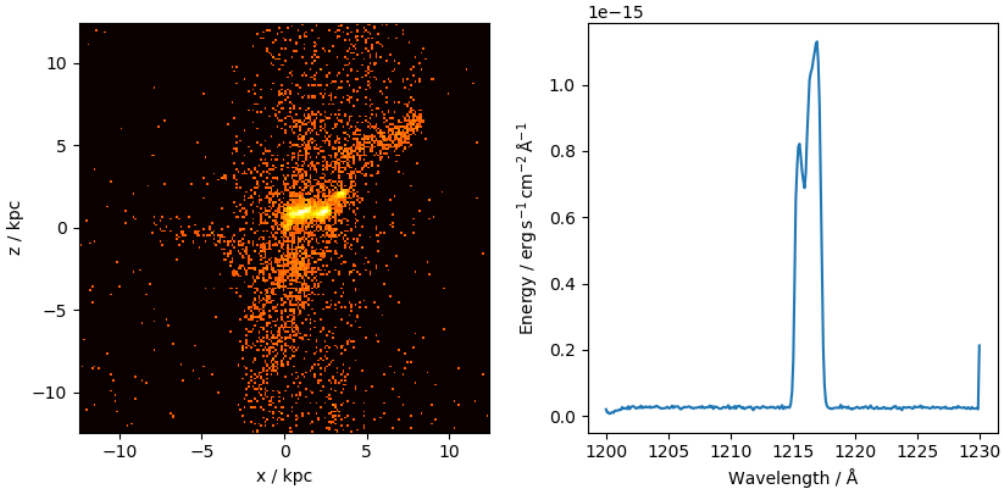

(b) Intrinsic Lyα surface brightness map and spectrum in negative y-direction.

Figure 4.8: Lyα surface brightness maps and spectra in the ym-direction. Shows the effect of Lyα photon scattering. The map covers surface brightnesses in the range $10^{-22} - 10^{-14}\,\mathrm{erg\,s\,cm^{-2}\,arcsec^{-2}}$.

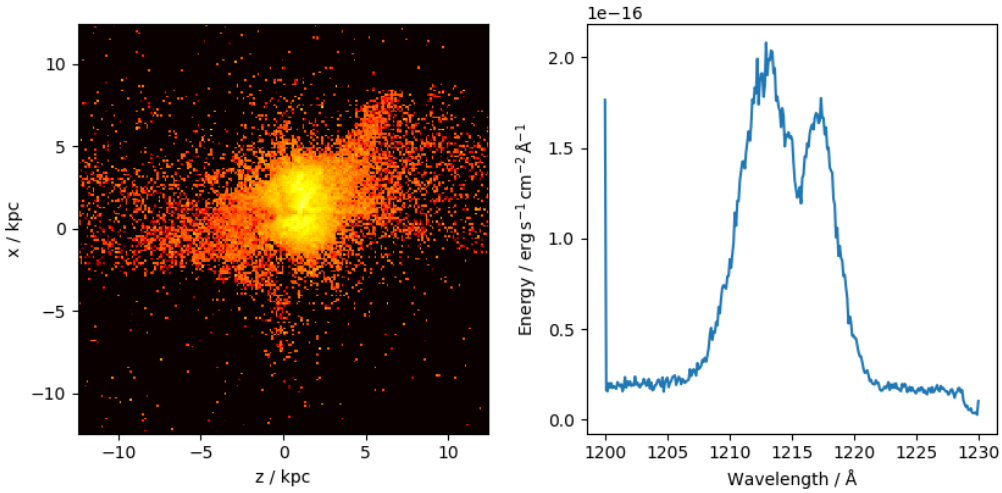

(a) Scattered Lyα surface brightness map and spectrum in positive y-direction.

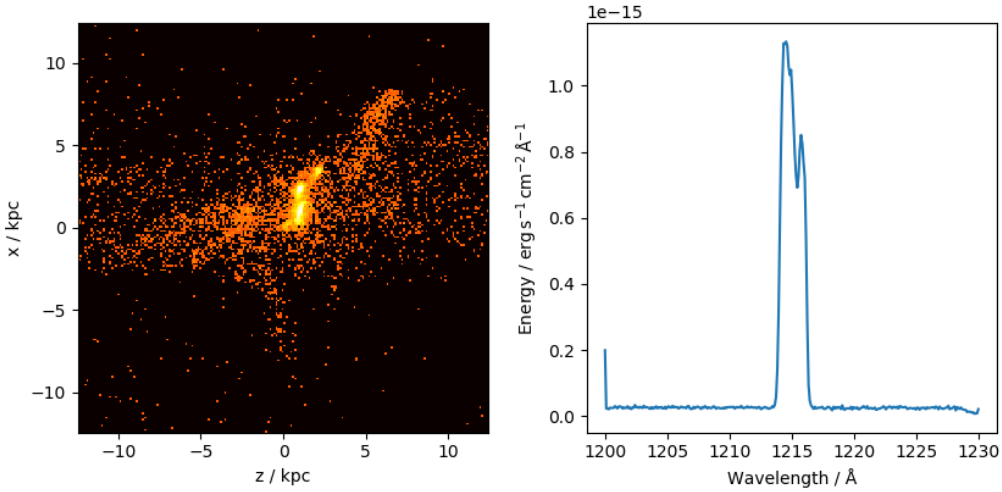

(b) Intrinsic Lyα surface brightness map and spectrum in positive y-direction.

Figure 4.9: Lyα surface brightness maps and spectra in the yp-direction. Shows the effect of Lyα photon scattering. The map covers surface brightnesses in the range $10^{-22} - 10^{-14}\,\mathrm{erg\,s\,cm^{-2}\,arcsec^{-2}}$.

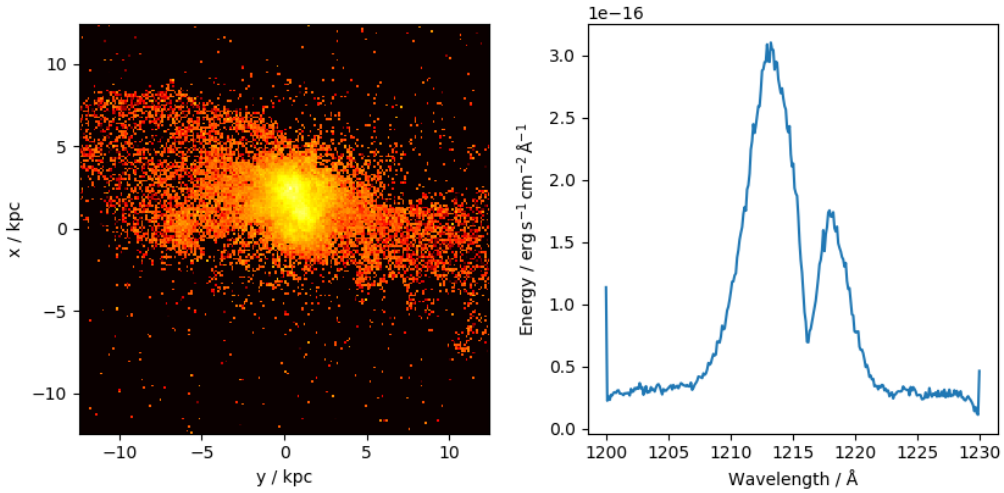

(a) Scattered Lyα surface brightness map and spectrum in negative z-direction.

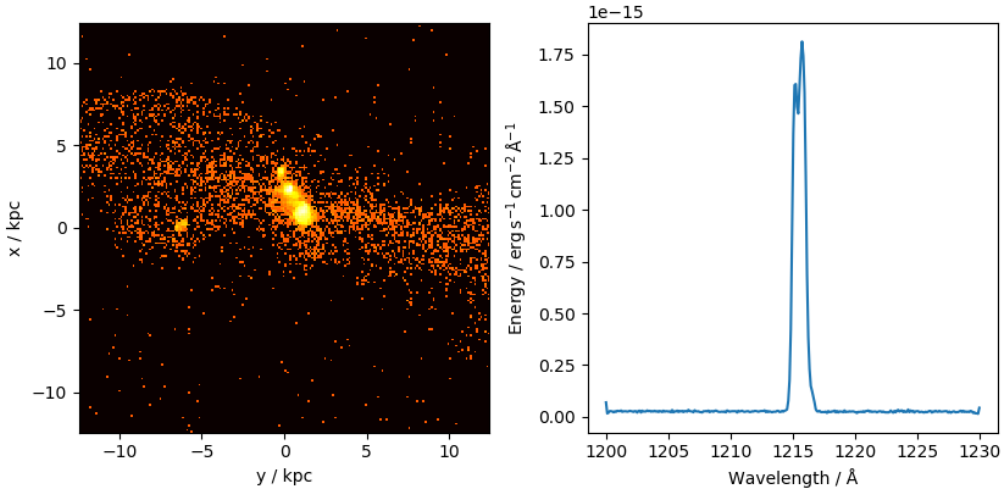

(b) Intrinsic Lyα surface brightness map and spectrum in negative z-direction.

Figure 4.10: Lyα surface brightness maps and spectra in the zm-direction. Shows the effect of Lyα photon scattering. The map covers surface brightnesses in the range $10^{-22} - 10^{-14}\,\mathrm{erg\,s\,cm^{-2}\,arcsec^{-2}}$.

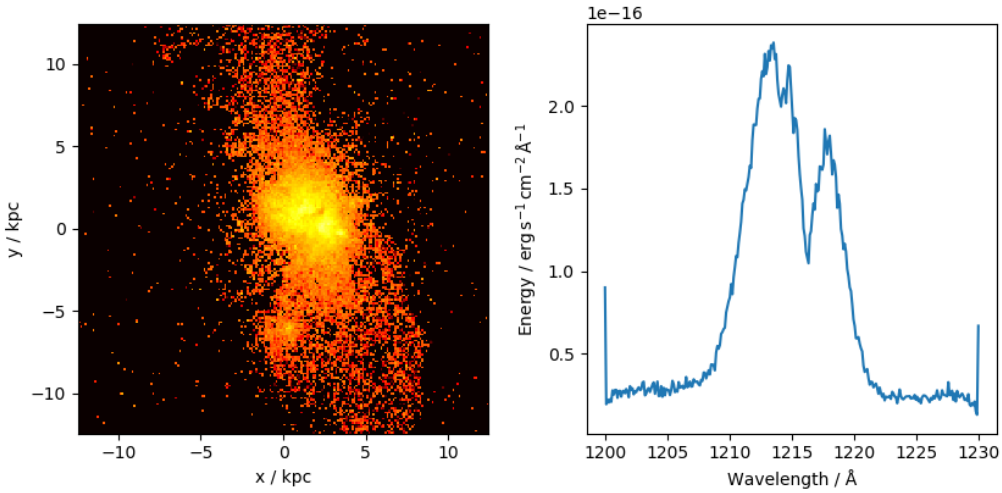

(a) Scattered Lyα surface brightness map and spectrum in positive z-direction.

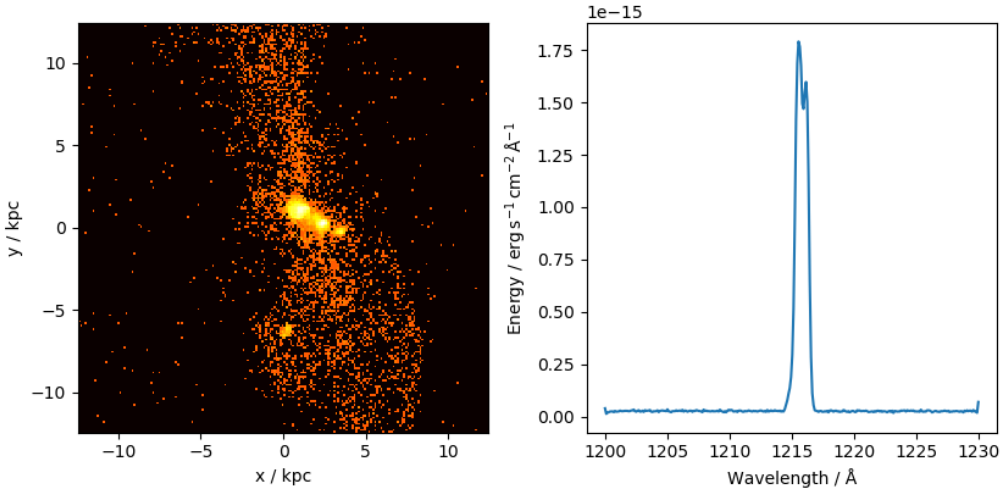

(b) Intrinsic Lyα surface brightness map and spectrum in positive z-direction.

Figure 4.11: Lyα surface brightness maps and spectra in the zp-direction. Shows the effect of Lyα photon scattering. The map covers surface brightnesses in the range $10^{-22} - 10^{-14}\,\mathrm{erg\,s\,cm^{-2}\,arcsec^{-2}}$.

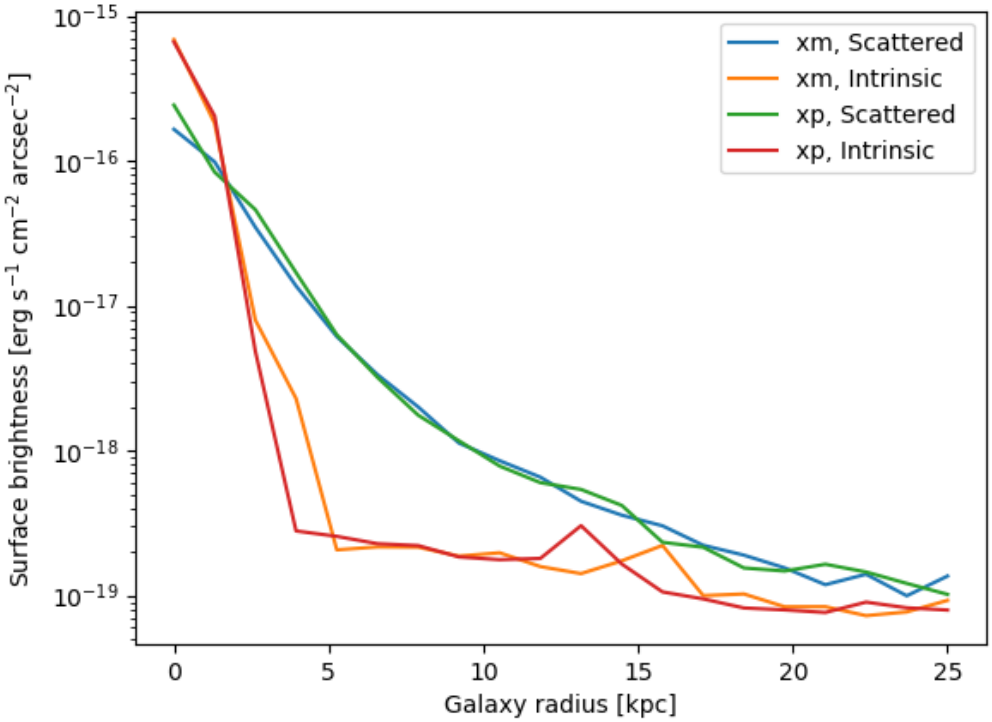

Figure 4.12: Surface brightness profile in both x-directions. Each profile is centred on the brightest pixel of the scattered profile of their specific direction, in a $200 \times 200\,\mathrm{pix}^2$ grid. For the xm direction this is pixel $(110, 108)$, 3.20 kpc from the galactic center. For the xp direction this is pixel $(107, 102)$, 1.82 kpc from the galactic center.

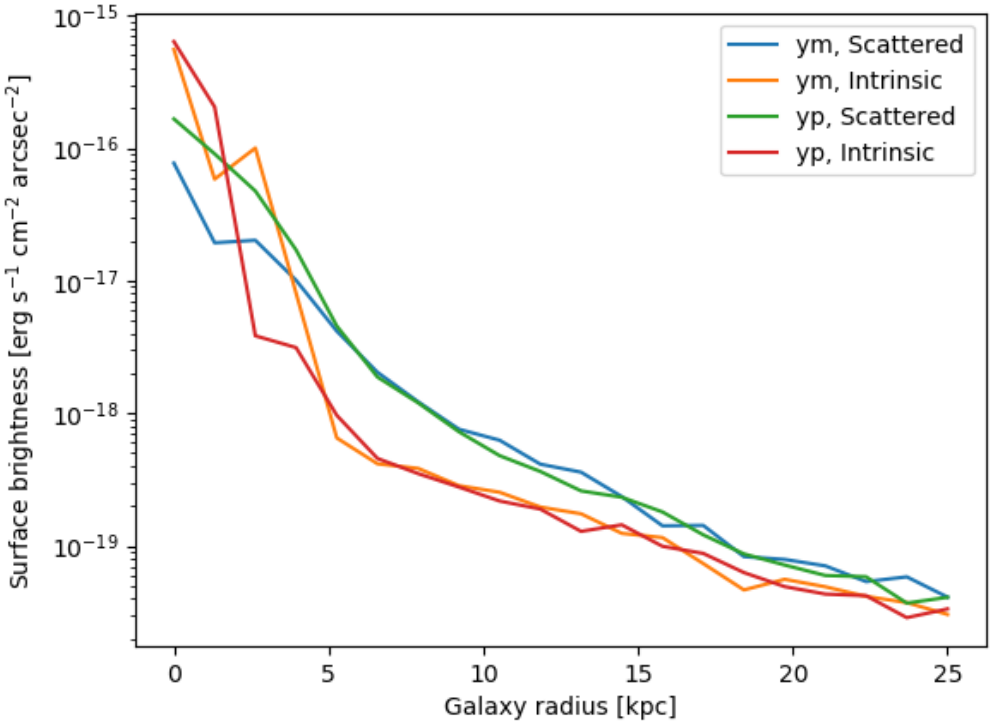

Figure 4.13: Surface brightness profile in both y-directions. Each profile is centred on the brightest pixel of the scattered profile of their specific direction, in a $200 \times 200\,\mathrm{pix}^2$ grid. For the ym direction this is pixel $(108, 119)$, 5.15 kpc from the galactic center. For the yp direction this is pixel $(110, 108)$, 3.20 kpc from the galactic center.

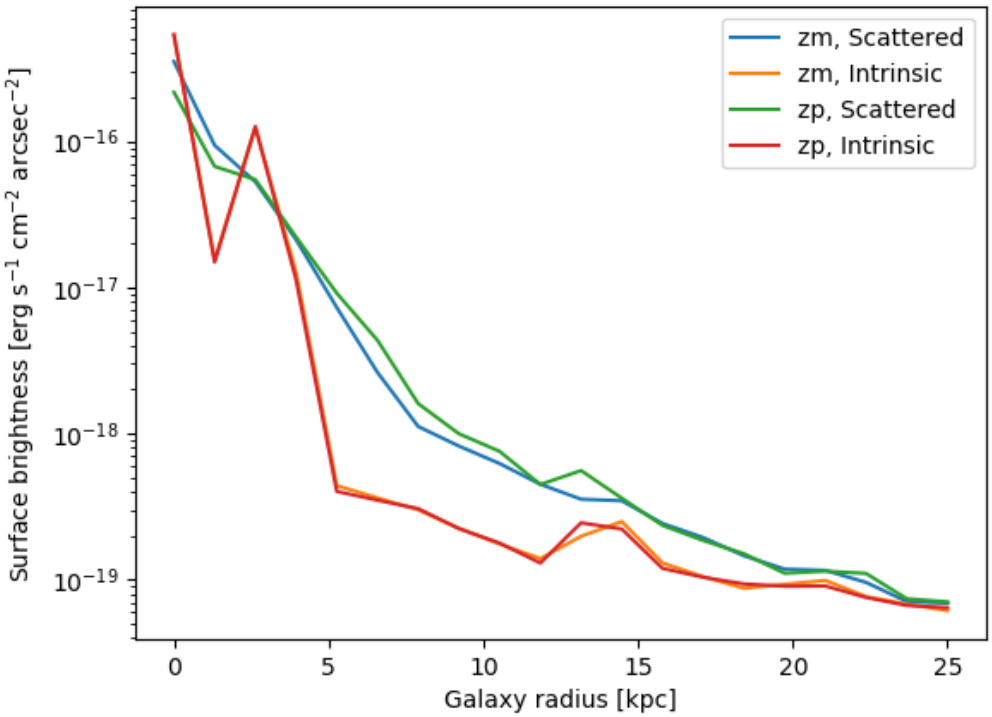

Figure 4.14: Surface brightness profile in both z-directions. Each profile is centred on the brightest pixel of the scattered profile of their specific direction, in a $200 \times 200\,\mathrm{pix}^2$ grid. For the zm direction this is pixel $(119, 102)$, 4.78 kpc from the galactic center. For the zp direction this is pixel $(101, 118)$, 4.51 kpc from the galactic center.

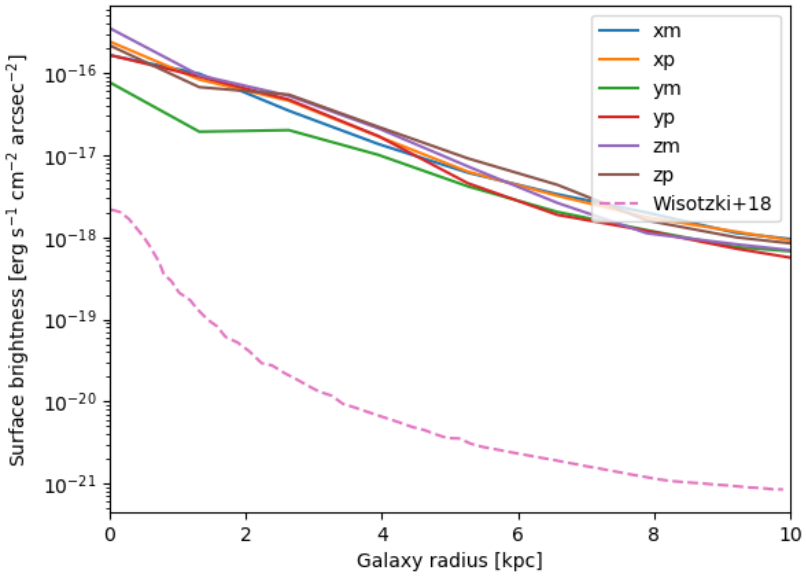

(a) Scattered Lyα surface brightnesses compared to redshift $5 < z < 6$ results from [5]. As [5] only reaches $r = 10\,\text{kpc}$, I also limit my plot to this for better visibility.

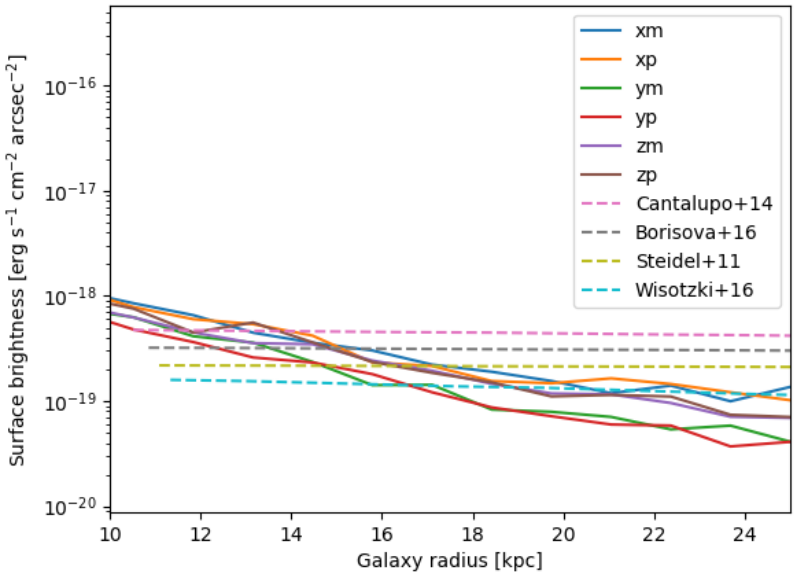

(b) Scattered Lyα surface brightness profile compared to [10], which collects data from [6], [7], [8] and [9]. As the figure I extracted this data from starts at $r = 10\,\text{kpc}$; I choose this as the starting point of this figure, and end it at my box radius $r = 25\,\text{kpc}$. The original observational curves went out to 100 kpc, which is why they are so flat in my figure.

Figure 4.15: Lyα surface brightness profiles compared to various observations. The observational data in figure 4.15a is from [5], while in figure 4.15b the curves are from [6], [7], [8] and [9]. These were collected in figure 9 in [10]. The curves have been extracted from the original plots using Web Plot Digitizer (`https://github.com/ankitrohatgi/WebPlotDigitizer`).

Chapter 5

Discussion and Conclusion

5.1 Galactic Parameters

Table 4.1 contains a plethora of parameters for the galaxy. The ones I included in the table are the "relevant" ones, that might be interesting to look at, and/or participates in my calculations. I have included the minimum, maximum and mean values of each parameter, as well as the sum for those where it makes sense. In most cases I use an accuracy of two decimals.

5.1.1 Recombination Luminosity

At the core of it all is the Lyα luminosity, as this the main parameter I am interested in studying. This has two main parts; luminosity from recombination and luminosity from cooling. I will talk about the cooling luminosity in subsection 5.1.2. When I talk about "luminosity" in other sections, it will be about the recombination luminosity unless otherwise mentioned.

The reason I am focusing on the Lyα luminosity is that this is the best visual indicator of a galaxy's properties. The luminosity has of units energy per time, so a snapshot of the luminosity tells us how much energy is produced at this very moment. This means the luminosity should change based on when we are looking at the galaxy. Looking at different kinds of luminosities will give information about ongoing processes in the galaxy. If a galaxy emits a lot of Lyα photons, for instance, we can gather that it contains a lot of ionized hydrogen. If it has less Lyα emission than a galaxy would usually have at that redshift and size, it could be an indicator of the galaxy containing a lot of dust that prevents the light from escaping, and so on.

Lyα radiation is, as mentioned earlier, the most abundant kind of light emitted by hydrogen atoms. This makes Lyα a great probe for galaxies at high redshifts, where other kinds of radiation might be too faint to detect.

A good way to check if I am on the right path to even finding the correct luminosity is to calculate it in two different ways. I have two available. First, there is equation 3.2, which gives an intrinsic luminosity of $L = 6.5 \times 10^{43}\,\mathrm{erg\,s^{-1}}$. Next, there is equation 2.6, the Kroupa IMF, which with an SFR of 41.42 gives $L = 7.04 \times 10^{43}\,\mathrm{erg\,s^{-1}}$. These

results are already very close, and the luminosity is expected to increase when the ionization schemes are applied. This is a good indication of the accuracy of my method, despite the many simplifications and rather crude approximations done along the way.

5.1.2 The Cooling Luminosity Conundrum

The recombination luminosity is looking well and good, but the cooling luminosity is another story entirely. Using equation 3.7, I get a total cooling luminosity of $L_{\text{cool,Ly}\alpha} = 2.11 \times 10^{45}\,\text{erg}\,\text{s}^{-1}$ (as seen in table 4.1). In other words, what should be 10% [39] of the recombination luminosity is instead 3376% of it. The conundrum is that this huge increase has no apparent source. All parameters of equation 3.7 have the right values. Figures 5.1 and 5.2 shows the same story, in that a transition happens at around $T = 10^4\,\text{K}$. Meanwhile, figure 5.3 shows a volume that (in the logarithmic plane) scales, for the most part, linearly with the hydrogen number density. In other words, there is nothing to suggest that any of the parameters are off.

Because of this, I choose not to use the cooling luminosity when I run through MoCaLaTA. It would be interesting in future works to see how the galaxy looks with it included, but for now, I simply can not solve it.

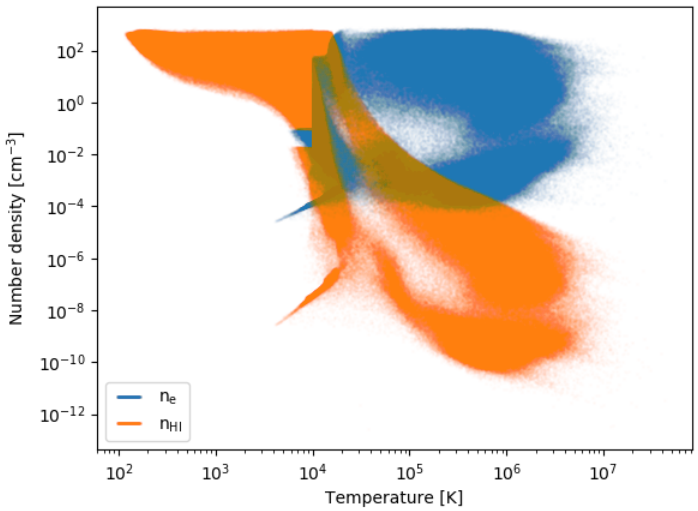

Figure 5.1: Number density of hydrogen and electrons as a function of temperature. This figure illustrates at what temperature the electrons start showing up, and when the neutral hydrogen disappears. The overlap would be where the hydrogen is partly ionized.

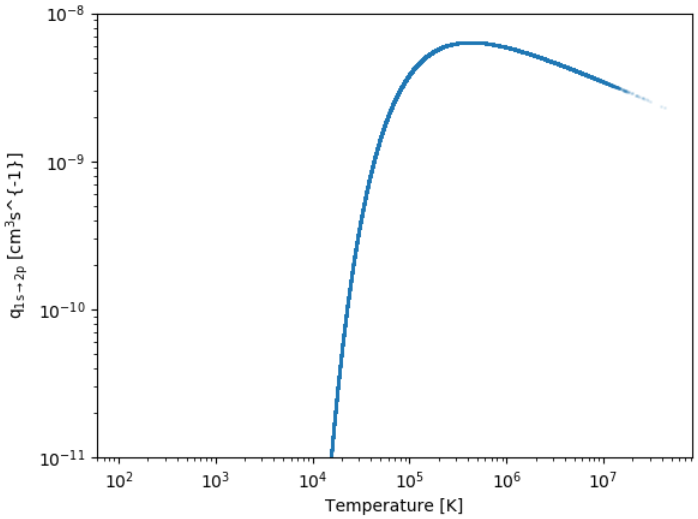

Figure 5.2: The collisional excitation rate coefficient (q-factor) as a function of temperature. Converges heavily towards zero as the gas gets colder.

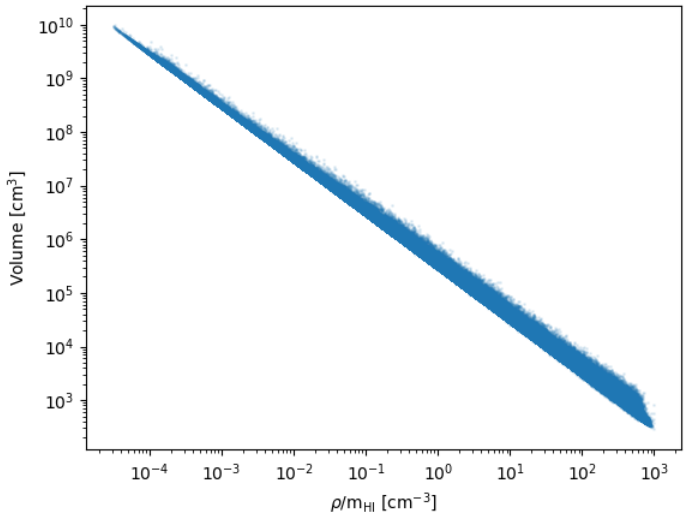

Figure 5.3: Volume of the gas particles as a function of hydrogen number density.

5.1.3 Mass and Star Formation

The star formation rate (SFR) and various component masses are given in table 4.2. Figure 4.3 shows how the star mass is doing in relation to the total halo mass, compared to other galaxies in the Universe.

The first thing that becomes apparent is that the relationship between star mass and halo mass is much higher than in other galaxies. Even comparing to redshift 5-6 galaxies, the Ponos galaxy is about half an order of magnitude higher, way outside the relevant error bar. This, along with other data, indicates I have a very high amount of stars in my galaxy.

As my method of calculating SFR comes directly from the masses of young stars, these quantities are numerically tied together. On the physics end of the spectrum, the large amount of young stars would exist due to the high SFR. Table 6 in [40] shows a "robust sample of 21 galaxies". The SFR based on the UV luminosity, with no dust correction, ranges from $3.8 - 16.4\,\mathrm{M}_\odot\,\mathrm{yr}^{-1}$. Compared to this my SFR is unusually high. Figure 4.4 also shows that when approaching the current redshift $z = 6.5$, the SFR grows massively, in what could be called an "starburst". Such bursts generally happen when the gas is cooling down and begins condensing. A good question then is what causes this cooling in the first place. I present two likely reasons:

(i) The Ponos simulation does not include enough feedback. Specifically, feedback from active galactic nuclei and radiative feedback from star formation are not in the simulation. Part of my project is to add this, but this will be after the SFR has already taken effect. Feedback processes are important for heating the gas, and without them it will naturally be cooler. One thing that is a bit sketchy with this explanation, though, is the fact that the starburst only happened very late in the galaxy's history. Lack of feedback should affect a long period of time, so while this may be part of the explanation, it does not necessarily paint the full picture.

(ii) Our dark matter halo had a merger with another halo. The large halos form when several small ones collide and merge. Our halo finder detected various halos in the simulation, and the one I am studying is simply the most prominent one. Based on the maps, another halo is very close to the main one, and it is entirely possible that they are merging. This would slow down the galaxies' angular momentums and cool them down significantly, thus giving us the starburst.

What can be discussed is how relevant the SFR *actually* is. A quick calculation with the code data shows that the young stars, defined to be younger than 35 million years old, comprise 28.5% of the total star mass. These are the same stars that are used for calculating the SFR. This is quite significant, the burst generates a lot of these stars. This might not necessarily mean much for the galaxy in the long run, as periods of high star formation wax and wane. However, if the lack of feedback is the issue, it should mean a lot when simulating down to lower redshifts. Therefore, it would be very interesting to see a version that goes down to lower redshift, to see whether the SFR is continuously high or if what we are witnessing is an exceptional peak. The former case would indicate that lack of feedback is the main culprit of the high SFR, while the latter would suggest a large halo merger.

5.2 Self-Shielding Approximations

As shown in table 4.3, the different self-shielding schemes give different results. Figure 4.5 shows which areas would be neutralized by each of the schemes. The important thing to take away from this is that a neutralized area will remove all intrinsic Lyα emission from that area. This essentially means that this area will emit no inherent radiation, and that cutting away large swathes of area will dramatically reduce the luminosity of the galaxy.

With this in mind, I look at the different schemes, and figure 4.5. Keeping the logarithmic x-axis in mind, it is clear that using any of the density-based schemes would remove emission from most gas in the galaxy. This is also clear from the numbers; looking at the data from the zoom-in box in table 4.3, the fine density shield would reduce the recombination Lyα luminosity to 0.1% of the original value and the coarse to 0.003%. Having a self-shielding *that* strong seems unrealistic, so I abandon the pure density-shields. There is also a physical argument, in that the density shield would remove any luminosity generation from the upper right quadrant of figure 4.5. This portion of the gas is dense and hot, and thus much more liable to internal ionization than the rest of the simulation. Reasons for this density and temperature can be for example supernova feedback or just close proximity to the galactic center.

The temperature-shield, on the other hand, will reduce the Lyα luminosity to 20% of the original. This is a far more realistic value. However, an argument can be made that being cold is not necessarily reason alone for the gas to be shielded. As seen in the lower left quadrant figure 4.5, there is a portion of gas particles that is cold, but not dense. This description fits the intergalactic medium well, which is not a large Lyα emitter. These properties makes the claim that the region is shielded seems a bit far-fetched. As table 4.3 shows, the numerical difference of excluding this quadrant from being shielded is pretty inconsequential, but the principle of the matter remains. Therefore, I declare in my code that the lower right quadrant of figure 4.5 - that is, where $n_{\mathrm{H}} > 0.1\,\mathrm{cm}^{-3}$ and $T < 10^4\,\mathrm{K}$ is entirely neutral, and does not produce, before application of ionization schemes, any recombination Lyα luminosity.

This is a very rough scheme, and misses out on some nuances. As mentioned earlier, the prime one being ionization from within the shield's borders. I do apply ionization form stars and from the AGN, but other potential sources, such as supernovae, are ignored. With this in mind I move on to the ionization schemes.

5.3 Interpolation

An important step in the project is interpolation from a particle-based SPH code in Python into a grid-based code in Fortran. The interpolation scheme is quite simple; I limit the SPH to the particles that would be inside my pre-determined box, count the number of particles in each cell and add their values. The two directly addable quantities are star mass for calculating the SFR and gas mass for calculating the mass density ρ. The others are weighted by mass.

In the appendix I present comparisons between the original values and the interpolated ones. As one can see, most of them fit to a satisfactory degree. The big, obvious exception is the mass density ρ. I have not been able to determine why this happens, and it does present us with a rather interesting scenario.

The Lyα luminosity in my box for the SPH is $L_{\text{SPH}} = 6.25 \times 10^{43}\,\text{erg}\,\text{s}^{-1}$. However, after interpolation, it is down to $L_{\text{grid}} = 1.60 \times 10^{43}\,\text{erg}\,\text{s}^{-1}$. The luminosity does, as per equation 3.2 use n_{e} and n_{HI} as terms. The $\alpha_B(T)$ is a function of temperature, which is neatly integrated, and the volume is a constant in each cell. Both n_{e} and n_{HI} are ρ-dependants, however, the latter which has shown to be rather sketchy after the interpolation. The evidence thus points to ρ as the culprit. Despite this, however, applying the - admittedly very aggressive - star ionization brings it back up again to $L = 7.69 \times 10^{43}\,\text{erg}\,\text{s}^{-1}$. This number happens to be close to the theoretical value one should get with our SFR - $L = 7.04 \times 10^{43}\,\text{erg}\,\text{s}^{-1}$.

The big question here is why. Are we just lucky, or is it deliberate based on the formulas? In other words, does ρ not matter that much when the galaxy is as heavily ionized as ours are?

The star ionization works by changing the mass fraction of neutral hydrogen f_{HI}. This again changes the mass fraction of HII through $f_{\text{HII}} = 0.764 - f_{\text{HI}}$, with 0.764 begin a cosmologically decided total hydrogen fraction. Looking at equation 3.1, we see that the number density is a function of the mass fraction and the mass density, both to first order. Thus one should not be much more important than the other.

Still, the end result is what we should expect for a galaxy with this SFR. That should mean something is working.

5.4 Ionizing the Gas

One thing missing from the initial version of the simulation is the ionization that stars and the AGN provides. An AGN is presumed to exist, as this is a very high-redshift galaxy, and would be very young.

To alleviate this I run ionization schemes presented in [10]. The star ionization comes from changing the neutral hydrogen mass fraction based on the ionizing radiation the gas would get from nearby stars, and the AGN ionization comes from simply declaring that everything within a certain radius of the galaxy is fully ionized.

First, I wish to discuss the AGN ionization. An inherent weakness in the method I use is that by using a purely radius-based scheme AGN jets are not taken into account. It is also binary, and does not partially ionize anything.

Ultimately, as seen in table 4.4, the AGN radius does not matter a whole lot unless extended to cover the entire virial radius. This result surprises me; I would have thought ionizing everything would have a bigger effect on the Lyα luminosity. A way to interpret this is that the gas is already pretty ionized, but if that was the case, the star ionization should not have such a comparatively large effect. What I take away from this is that the gas around the *center* must be very ionized already, and therefore applying more through the AGN does not do much. The star ionization however affects the whole

galaxy, and therefore ionizes the areas the centralized AGN will not reach.

This claim can be disputed by pointing out that the star formation would also occur mostly close to the center. Perhaps this boost in Lyα comes from star formation in the other two smaller galaxies?

The ionization processes gives a final luminosity higher than normal for high-redshift galaxies, and makes it apt to compare with superluminous Lyα nebulae [10], as discussed in 5.5.1.

5.5 Scattering and MoCaLaTA

Looking at the MoCaLaTA results and the scattering gives the image that is most true to what one would actually observe. The spectra in figures 4.6 through 4.11 are aligned with the theory that most escapes happen when photons are Doppler shifted. A notable figure with the intrinsic spectra is that they are more or less identical in the positive and negative directions along the same axis. Since the initial photon emission (before any scattering is applied) is completely random, this is natural. The small differences are easily explained as random occurrences based on photon resolution N_γ. If more photons were emitted, the spectra and surface brightness profiles both should be identical.

Moving on to the surface brightness maps, the effects of the scattering is stunning. The light is much more smeared out, and the effect gas has on the radiation is clearly represented. The intrinsic images - especially zp - show the same picture as figure 4.2. The scattering reveals a whole other picture, with the details smeared out, but the image looking much more like what we would see through the a telescope. The main reason I am interested in the scattering, however, is because of the surface brightness profiles.

Figure 4.12, 4.13 and 4.14 shows the surface brightness profiles (SBP) in the x, y and z-directions respectively. These gives a picture of how the surface brightness changes as a function of the galaxy radius. The way this works is by creating small shells at certain radial intervals, summing up the luminosity between this shell and the previous, and plotting it as a function of the shell's radius.

It is important to note that the SBPs do not start in the same pixel. As my intention is to compare the SBPs to observations, starting at the galactic centre would, while realistic, be detrimental to this purpose. When observing a galaxy it is common to declare that the brightest visible spot is the center. While scattering makes so that this is not necessarily true, it is the best method available, and is "close enough". Therefore I start each of my curves in different pixels. Their distances from the galactic center are shown in table 4.5. This ensures that any of the six directions from which my galaxy is observable could be the direction facing the Earth - if the galaxy was real, of course.

Along with the scattered surface brightnesses I have included the intrinsic ones. They have three notable traits:

(i) They start at higher values than the scattered SBPs.

(ii) They quickly gain lower values than the scattered SBPs.

(iii) They are more fractured/less smooth than their scattered counterparts.

These can all be explained by the scattering evening out the SBPs. Intrinsically, the vast majority of the Lyα photons would - as with all galactic radiation - come from the galactic center. The scattering will to a certain degree smooth this out, by having the photons bounce around in the galaxy before escaping. Do note that there is still a difference of three orders of magnitude in the scattered SBPs - the Lyα radiation from the center is still 1000 times stronger than from the edges. It is just not *as* extreme an difference as the four orders of magnitude we see in some of the intrinsic SBPs. The scattered image *should* be smoother, which it is.

Table 4.5 also shows that the escaped flux is in general larger for the intrinsic model, in one case over six times as large. The main reason is that the photons are scattered out of the line of sight. Looking at the data log, only 71% of the photons escaped after being scattered, compared to 98% in the intrinsic case.

5.5.1 Comparison to Observations

The main point of the SBPs are, as mentioned earlier, to compare with observations. I have done this in figure 4.15.

After first comparing to [5], where I specifically compare to figure 2c for redshift $5 < z < 6$, it quickly becomes apparent that my galaxy is **much** brighter than the ones I compare to. This is in line with the abnormally high SFR observed earlier. Being 100 times more luminous than could be expected from other galaxies of similar redshifts, I instead move on to compare to the data collected and presented by [10]. My data is a much better fit for these observation, and shows the Ponos galaxy as superluminous.

The reason the luminosity goes so high is because of the very high SFR. The most likely reason for this is due to galaxy mergers. The heating from supernovae and stellar radiation ionizes gas in the ISM and CGM; and when this gas recombines it gives a Lyα luminosity comparable to the giant Lyα nebulae.

This opens up an interesting avenue for detection of Lyα emission in the "cosmic dawn", where $z > 6$. Superluminous objects have traditionally been rare, but since mergers are common in the high-redshift Universe, they may not be as uncommon as people initially suspected. Nevertheless, this superluminosity might be very temporary. As soon as the galaxy merger is finished and the feedback disperses the condensing gas it causes the galaxy might go back down again to expected emission values. The rarity of observing superluminous objects would remain, as the small temporary ones would not retain their superluminosity for long.

The veracity of this claim has yet to be confirmed, as we would need more investigations and samples.

5.6 Conclusion

The main conclusion I have arrived to, through studying luminosity and surface brightness, is that the Ponos simulation is indeed able to replicate observed celestial objects. The plot twist, however, is that instead of having similar surface brightness profiles to high-redshift galaxies, Ponos fits much better with giant Lyα nebulae.

I believe the abnormally high star formation rate to be at the core of this. Almost 30% of the stars in Ponos are younger than 35 Myr (assume all stars have the same mass), related to the huge star formation peak (starburst) that begins around 150 million years before our $z = 6.5$ snapshot (as seen in figure 4.4).

I have two postulates for why the SFR gets so high. The first is from lack of AGN and stellar radiation feedback. Feedback cools the gas, increasing the SFR. The second, that I find more likely, is that is that there may have been a halo collision at the time where the SFR starts to peak. There are numerous dark matter haloes in the simulation, and figure 4.2 shows that a lesser galaxy is on the way into the main one. A collision would reduce the angular momentum of the gas, which would make it condense and cool, thus enabling star formation.

This leads to superluminosity, giving the Ponos simulation a luminosity many times higher than what its mass would suggest. Due to how common galaxy mergers are in the early Universe, this might mean superluminous objects are not as rare as we think. The superluminosity is however likely to be temporary; explaining why not more of these objects have been observed.

5.6.1 Future Work

1. My first suggestion for future work in this field is to investigate the same simulation at lower redshifts. This way we it can be checked whether the superluminosity drops again after the starburst; or is a permanent feature of the simulation. This could also give a better indication on whether the galaxy merger is indeed the reason for the starburst, or if lack of feedback is the culprit.

2. While the version of Ponos I have looked at has a high resolution, there exist an even higher-resolution version. It would be very interesting to see if we see the same phenomena in this one.

3. Speaking of resolution, higher resolution could also be tried for runs of MoCaLaTA. As this was amongst the final things I did in this project, I regretfully did not have the time to run MoCaLaTA with the photon resolution the project deserved. I am regardless happy with the images I got, but would be very interested to see a runs with even higher resolution.

4. All my results are also based on the assumption that the light shown in my maps is actually the light that would hit us at Earth. I ignore the fact that there is a lot of gas in between, in the form of the intergalactic medium. A good study for the future would be to see how this affects the luminosity.

5. Last of all, there are of course other simulations out there, with different halos at different redshifts. It would be interesting to see similar analyses done on them, to see if the starburst-superluminosity relation is a repeating trend, or something specifically done by Ponos.

Appendices

Appendix A

Appendix

In going from an SPH to a grid code, I did a manual interpolation of the values. In order to see that the interpolation worked sufficiently, I made histograms for the values of the SPH and the newly interpolated grid values, side by side. In this appendix I present them, if it is in the reader's interest to see the comparison for themselves. Each histogram had to be custom made, as different methods were used to show the best comparative image.

In summary, every value except for the mass density had a seemingly good interpolation. However, this does not seem to matter much, as the final results are still solid.

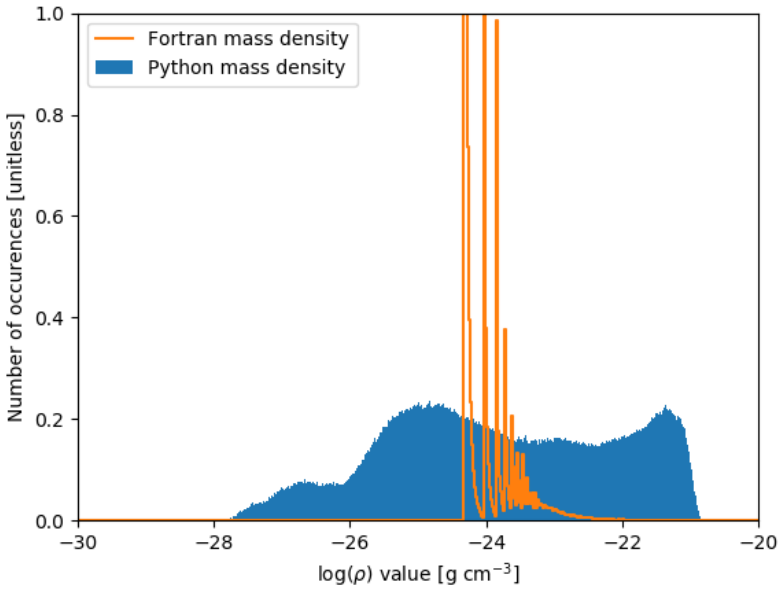

(a) Mass density ρ. Logarithmic, normalized.

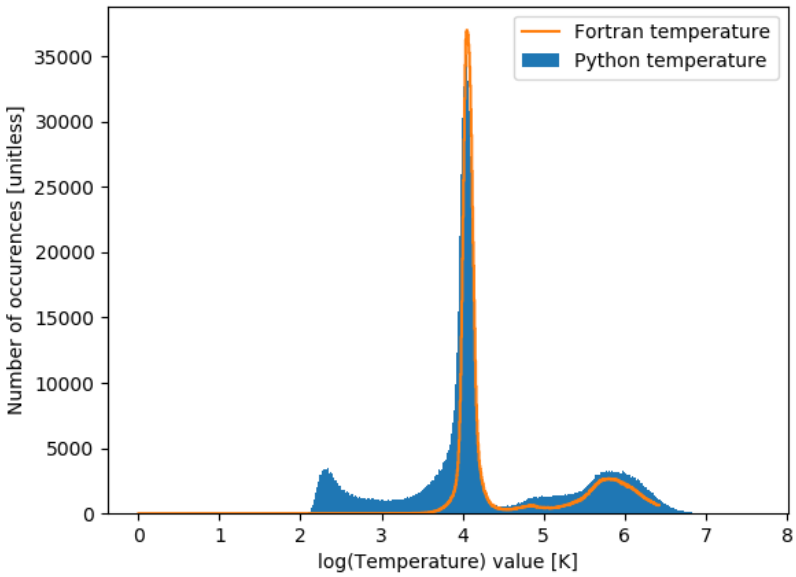

(b) Temperature T. Logarithmic, unnormalized.

Figure A.1: Density and temperature interpolation comparisons.

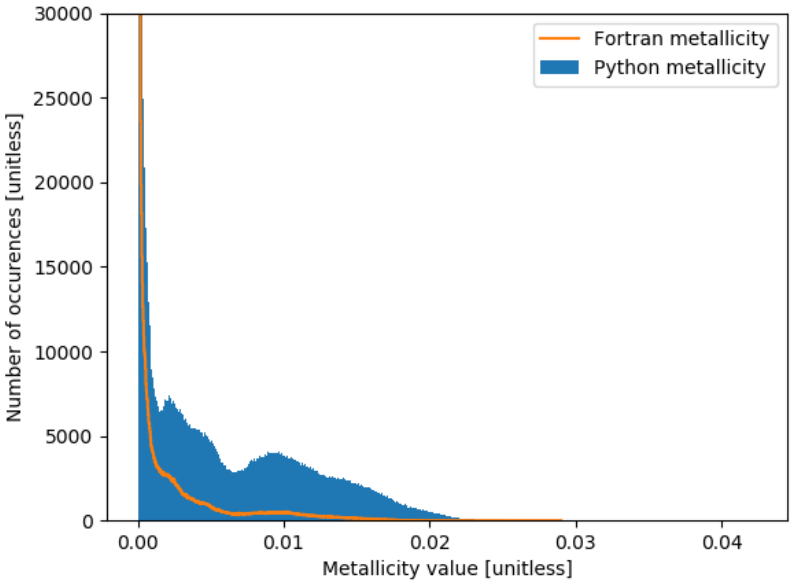

(a) Metallicity f_{metals}. Linear, unnormalized.

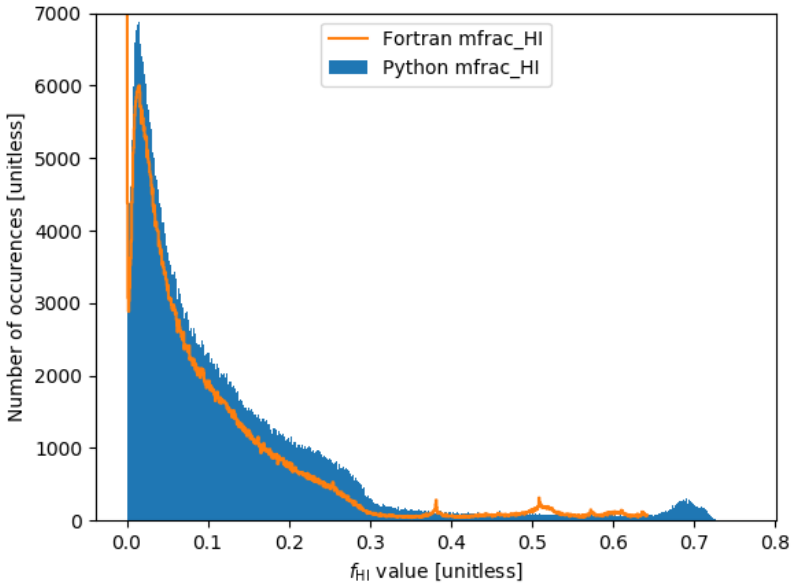

(b) Mass fraction of neutral hydrogen f_{HI}. Linear, unnormalized.

Figure A.2: Metallicity and HI mass fraction interpolation comparisons.

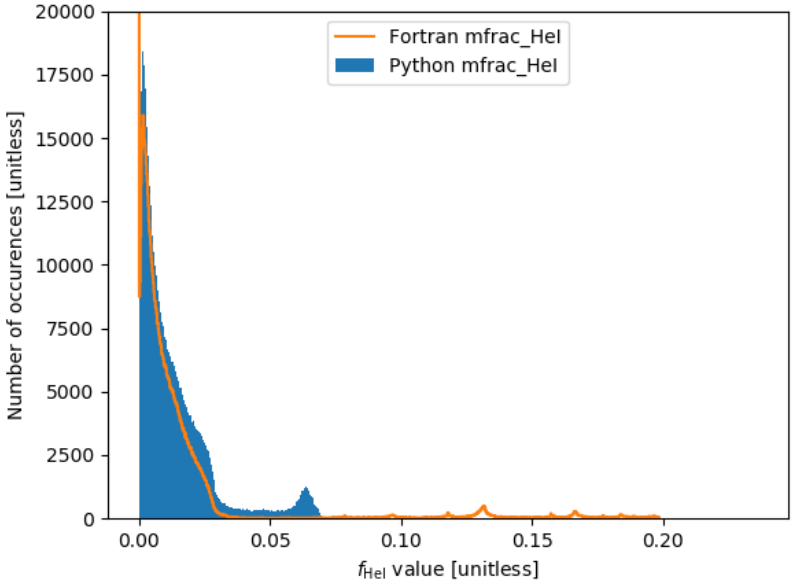

(a) Mass fraction of neutral helium f_{HeI}. Linear, unnormalized.

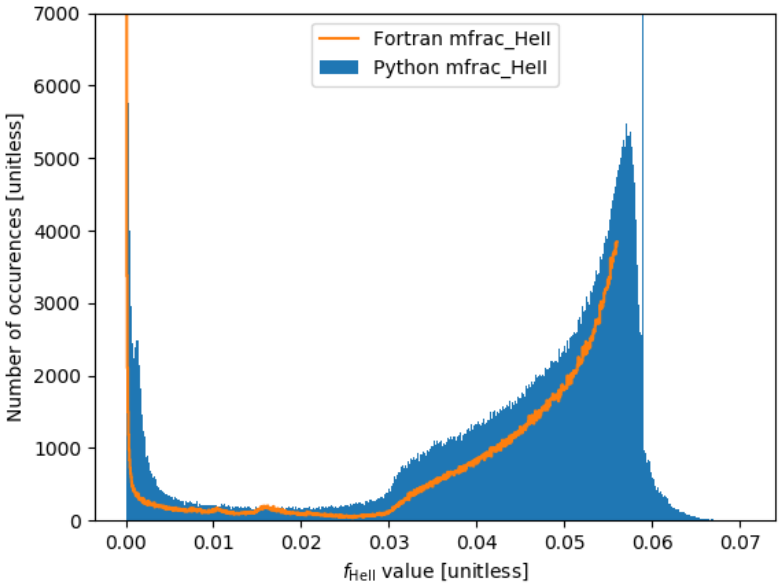

(b) Mass fraction of singularly ionized helium f_{HeII}. Linear, unnormalized.

Figure A.3: Helium mass fraction interpolation comparisons.

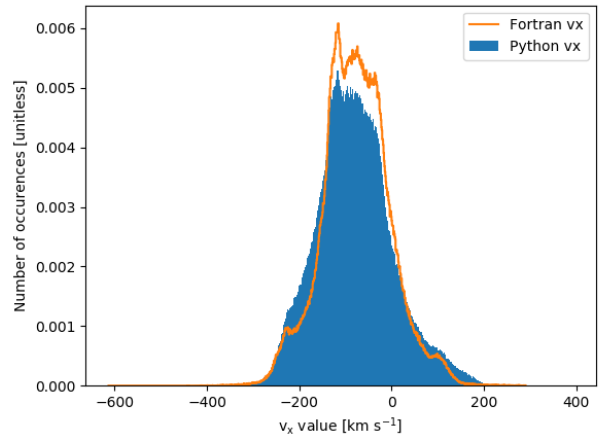

(a) Velocity in x-direction v_{x}. Linear, normalized.

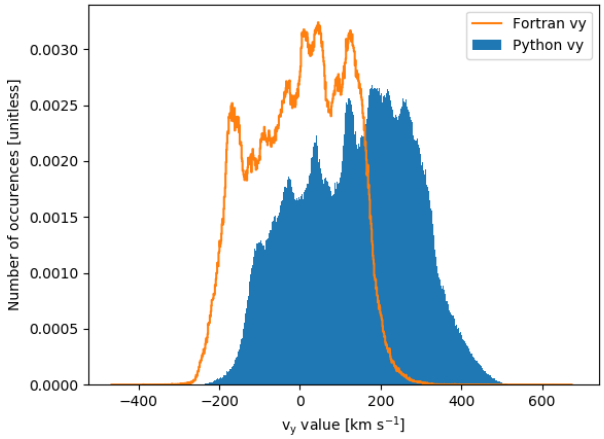

(b) Velocity in y-direction v_{y}. Linear, normalized.

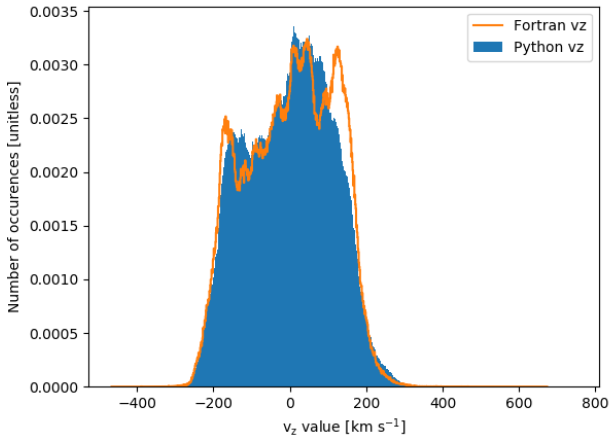

(c) Velocity in z-direction v_{z}. Linear, normalized.

Figure A.4: Velocity interpolation comparisons.

Bibliography

[1] Mark Dijkstra. Saas-Fee Lecture Notes: Physics of Lyman Alpha Radiative Transfer. *none*, 2017.

[2] Peter Laursen. Lymanα radiative transfer in the high-redshift, dusty Universe. *arXiv e-prints*, page arXiv:1012.3175, Dec 2010.

[3] Daniel J. Price. SPLASH: An interactive visualisation tool for Smoothed Particle Hydrodynamics simulations. *Publ. Astron. Soc. Austral.*, 24:159, 2007.

[4] P. S. Behroozi, R. H. Wechsler, and C. Conroy. The Average Star Formation Histories of Galaxies in Dark Matter Halos from z = 0-8. *apj*, 770:57, June 2013.

[5] L. Wisotzki, R. Bacon, J. Brinchmann, S. Cantalupo, P. Richter, J. Schaye, K. B. Schmidt, T. Urrutia, P. M. Weilbacher, M. Akhlaghi, N. Bouché, T. Contini, B. Guiderdoni, E. C. Herenz, H. Inami, J. Kerutt, F. Leclercq, R. A. Marino, M. Maseda, A. Monreal-Ibero, T. Nanayakkara, J. Richard, R. Saust, M. Steinmetz, and M. Wendt. Nearly all the sky is covered by Lyman-α emission around high-redshift galaxies. *nat*, 562(7726):229–232, Oct 2018.

[6] Sebastiano Cantalupo, Fabrizio Arrigoni-Battaia, J. Xavier Prochaska, Joseph F. Hennawi, and Piero Madau. A cosmic web filament revealed in Lyman-α emission around a luminous high-redshift quasar. *nat*, 506:63–66, February 2014.

[7] Elena Borisova, Sebastiano Cantalupo, Simon J. Lilly, Raffaella A. Marino, Sofia G. Gallego, Roland Bacon, Jeremy Blaizot, Nicolas Bouché, Jarle Brinchmann, C. Marcella Carollo, Joseph Caruana, Hayley Finley, Edmund C. Herenz, Johan Richard, Joop Schaye, Lorrie A. Straka, Monica L. Turner, Tanya Urrutia, Anne Verhamme, and Lutz Wisotzki. UBIQUITOUS GIANT lyαNEBULAE AROUND THE BRIGHTEST QUASARS ATz$\sim$ 3.5 REVEALED WITH MUSE. *The Astrophysical Journal*, 831(1):39, oct 2016.

[8] Charles C. Steidel, Milan Bogosavljević, Alice E. Shapley, Juna A. Kollmeier, Naveen A. Reddy, Dawn K. Erb, and Max Pettini. DIFFUSE lyα EMITTING HALOS: A GENERIC PROPERTY OF HIGH-REDSHIFT STAR-FORMING GALAXIES. *The Astrophysical Journal*, 736(2):160, jul 2011.

[9] L. Wisotzki, R. Bacon, J. Blaizot, J. Brinchmann, E. C. Herenz, J. Schaye, N. Bouché, S. Cantalupo, T. Contini, C. M. Carollo, J. Caruana, J. B. Courbot, E. Emsellem, S. Kamann, J. Kerutt, F. Leclercq, S. J. Lilly, V. Patrício, C. Sandin, M. Steinmetz, L. A. Straka, T. Urrutia, A. Verhamme, P. M. Weilbacher, and M. Wendt. Extended Lyman α haloes around individual high-redshift galaxies revealed by MUSE. *aap*, 587:A98, Mar 2016.

[10] Max Gronke and Simeon Bird. Giant Lyman-alpha Nebulae in the Illustris Simulation. *apj*, 835:207, February 2017.

[11] R. B. Partridge and P. J. E. Peebles. Are Young Galaxies Visible? *apj*, 147:868, March 1967.

[12] A. Zitrin, A. Fabris, J. Merten, P. Melchior, M. Meneghetti, A. Koekemoer, D. Coe, M. Maturi, M. Bartelmann, M. Postman, K. Umetsu, G. Seidel, I. Sendra, T. Broadhurst, I. Balestra, A. Biviano, C. Grillo, A. Mercurio, M. Nonino, P. Rosati, L. Bradley, M. Carrasco, M. Donahue, H. Ford, B. L. Frye, and J. Moustakas. Hubble Space Telescope Combined Strong and Weak Lensing Analysis of the CLASH Sample: Mass and Magnification Models and Systematic Uncertainties. *apj*, 801:44, March 2015.

[13] Pavel Kroupa. The initial mass function and its variation. *ASP Conf. Ser.*, 285:86, 2002.

[14] Craig J. Hogan and Ray J. Weymann. Lyman-alpha emission from the Lyman-alpha forest. *Monthly Notices of the Royal Astronomical Society*, 225(1):1P–5P, 03 1987.

[15] A. Gould and D. H. Weinberg. Imaging the Forest of Lyman Limit Systems. *apj*, 468:462, September 1996.

[16] Donald R. Hamilton. On directional correlation of successive quanta. *Phys. Rev.*, 58:122–131, Jul 1940.

[17] J. O. Stenflo. Resonance-line polarization. V - Quantum-mechanical interference between states of different total angular momentum. *aap*, 84:68–74, April 1980.

[18] D. E. Osterbrock. The Escape of Resonance-Line Radiation from an Optically Thick Nebula. *apj*, 135:195, January 1962.

[19] Primarch of the Salamanders Vulkan. Only War. *Warhammer 40,000*, War of the Beast, 31500.

[20] A. Pontzen, R. Roškar, G. Stinson, and R. Woods. pynbody: N-Body/SPH analysis for python. Astrophysics Source Code Library, May 2013.

[21] Davide Fiacconi, Lucio Mayer, Piero Madau, Alessandro Lupi, Massimo Dotti, and Francesco Haardt. Young and turbulent: the early life of massive galaxy progenitors. *Mon. Not. Roy. Astron. Soc.*, 467(4):4080–4100, 2017.

[22] R. A. Gingold and J. J. Monaghan. Smoothed particle hydrodynamics - Theory and application to non-spherical stars. *mnras*, 181:375–389, November 1977.

[23] L. B. Lucy. A numerical approach to the testing of the fission hypothesis. *aj*, 82:1013–1024, December 1977.

[24] J.W. Wadsley, J. Stadel, and T. Quinn. Gasoline: a flexible, parallel implementation of treesph. *New Astronomy*, 9(2):137 – 158, 2004.

[25] S. Shen, J. Wadsley, and G. Stinson. The enrichment of the intergalactic medium with adiabatic feedback - I. Metal cooling and metal diffusion. *Monthly Notices of the Royal Astronomical Society*, 407(3):1581–1596, 09 2010.

[26] Francesco Haardt and Piero Madau. Radiative Transfer in a Clumpy Universe. IV. New Synthesis Models of the Cosmic UV/X-Ray Background. *apj*, 746(2):125, Feb 2012.

[27] Greg Stinson, Anil Seth, Neal Katz, James Wadsley, Fabio Governato, and Tom Quinn. Star formation and feedback in smoothed particle hydrodynamic simulations - I. Isolated galaxies. *Monthly Notices of the Royal Astronomical Society*, 373(3):1074–1090, 11 2006.

[28] E. Komatsu, K. M. Smith, J. Dunkley, C. L. Bennett, B. Gold, G. Hinshaw, N. Jarosik, D. Larson, M. R. Nolta, L. Page, D. N. Spergel, M. Halpern, R. S. Hill, A. Kogut, M. Limon, S. S. Meyer, N. Odegard, G. S. Tucker, J. L. Weiland, E. Wollack, and E. L. Wright. SEVEN-YEARWILKINSON MICROWAVE ANISOTROPY PROBE(WMAP) OBSERVATIONS: COSMOLOGICAL INTERPRETATION. *The Astrophysical Journal Supplement Series*, 192(2):18, jan 2011.

[29] G. Hinshaw, D. Larson, E. Komatsu, D. N. Spergel, C. L. Bennett, J. Dunkley, M. R. Nolta, M. Halpern, R. S. Hill, N. Odegard, L. Page, K. M. Smith, J. L. Weiland, B. Gold, N. Jarosik, A. Kogut, M. Limon, S. S. Meyer, G. S. Tucker, E. Wollack, and E. L. Wright. Nine-year Wilkinson Microwave Anisotropy Probe (WMAP) Observations: Cosmological Parameter Results. *apjs*, 208:19, October 2013.

[30] Ji hoon Kim, Tom Abel, Oscar Agertz, Greg L. Bryan, Daniel Ceverino, Charlotte Christensen, Charlie Conroy, Avishai Dekel, Nickolay Y. Gnedin, Nathan J. Goldbaum, Javiera Guedes, Oliver Hahn, Alexander Hobbs, Philip F. Hopkins, Cameron B. Hummels, Francesca Iannuzzi, Dusan Keres, Anatoly Klypin, Andrey V. Kravtsov, Mark R. Krumholz, Michael Kuhlen, Samuel N. Leitner, Piero Madau, Lucio Mayer, Christopher E. Moody, Kentaro Nagamine, Michael L. Norman, Jose Onorbe, Brian W. OShea, Annalisa Pillepich, Joel R. Primack, Thomas Quinn, Justin I. Read, Brant E. Robertson, Miguel Rocha, Douglas H. Rudd, Sijing Shen, Britton D. Smith, Alexander S. Szalay, Romain Teyssier, Robert Thompson,

Keita Todoroki, Matthew J. Turk, James W. Wadsley, John H. Wise, , and Adi Zolotov and. THE AGORA HIGH-RESOLUTION GALAXY SIMULATIONS COMPARISON PROJECT. *The Astrophysical Journal Supplement Series*, 210(1):14, dec 2013.

[31] Oliver Hahn and Tom Abel. Multi-scale initial conditions for cosmological simulations. *Monthly Notices of the Royal Astronomical Society*, 415(3):2101–2121, 08 2011.

[32] S. P. D. Gill, A. Knebe, and B. K. Gibson. The evolution of substructure - I. A new identification method. *mnras*, 351:399–409, June 2004.

[33] S. R. Knollmann and A. Knebe. AHF: Amiga's Halo Finder. *apjs*, 182:608–624, June 2009.

[34] L. Hui and N. Y. Gnedin. Equation of state of the photoionized intergalactic medium. *mnras*, 292:27, November 1997.

[35] S. Cantalupo, C. Porciani, and S. J. Lilly. Mapping Neutral Hydrogen during Reionization with the Lyα Emission from Quasar Ionization Fronts. *apj*, 672:48–58, January 2008.

[36] P. Laursen, A. O. Razoumov, and J. Sommer-Larsen. Lyα Radiative Transfer in Cosmological Simulations Using Adaptive Mesh Refinement. *apj*, 696:853–869, May 2009.

[37] Tobias Goerdt, A. Dekel, A. Sternberg, D. Ceverino, R. Teyssier, and J. R. Primack. Gravity-driven Lyα blobs from cold streams into galaxies. *Monthly Notices of the Royal Astronomical Society*, 407(1):613–631, 08 2010.

[38] Alireza Rahmati, Joop Schaye, Andreas H. Pawlik, and Milan Raicevic. The impact of local stellar radiation on the HI column density distribution. *Monthly Notices of the Royal Astronomical Society*, 431(3):2261–2277, 03 2013.

[39] Peter Laursen, Jesper Sommer-Larsen, Bo Milvang-Jensen, Johan P. U. Fynbo, and Alexei O. Razoumov. Chasing Lyman alpha-emitting galaxies at z = 8.8. *arXiv e-prints*, page arXiv:1806.07392, Jun 2018.

[40] R. J. McLure, J. S. Dunlop, L. de Ravel, M. Cirasuolo, R. S. Ellis, M. Schenker, B. E. Robertson, A. M. Koekemoer, D. P. Stark, and R. A. A. Bowler. A robust sample of galaxies at redshifts 6.0<z<8.7: stellar populations, star formation rates and stellar masses. *mnras*, 418(3):2074–2105, Dec 2011.